The Vertical Partition of Oceanic Horizontal Kinetic Energy

CARL WUNSCH

Department of Earth, Atmospheric and Planetary Sciences, Massachusetts Institute of Technology, Cambridge, Massachusetts

(Manuscript received 9 September 1996, in final form 13 February 1997)

ABSTRACT

To produce an interpretation of the surface kinetic energy as measured by altimeters, a survey is made of the vertical structure of kinetic energy profiles in a large number of globally distributed long current meter records. Although the data are geographically confined primarily to a latitude band in the North Pacific, to the North Atlantic, and to a few moorings in the South Atlantic, the results show, generally speaking, that most regions are dominated by the barotropic and first baroclinic modes. Because of the near-surface intensification of baroclinic modes altimeters primarily reflect the first baroclinic mode, and thus the motion of the main thermocline. There is good quantitative agreement, with a few exceptions, with estimates of the surface kinetic energy obtained from the TOPEX/POSEIDON altimeter and from vertical extrapolations to the surface of the mooring profiles. These results are consistent with previous suggestions that barotropic models have little skill in depicting variability as seen in the altimeter data. An EOF analysis is shown to produce fictitious mode coupling unless the dynamical modes have very different energy levels.

1. Introduction

The vertical partitioning of oceanic kinetic energy into barotropic and baroclinic components is an important descriptive feature of the large-scale ocean circulation. Apart from the issue of describing and explaining the observed distribution, this vertical structure is an essential element in understanding altimetric measurements of sea surface elevation and slope. In a previous paper, Wunsch and Stammer (1995) presented an estimate obtained from the altimetric data of the TOPEX/POSEIDON mission of the frequency–wavenumber power spectrum of the time variability of the general circulation as reflected in the surface and surface slope variability. Subsequently, Stammer (1997) broke the global spectrum down into regional elements. This present paper is directed at understanding the vertical partitioning of kinetic energy in the ocean with the aim of producing a full three-dimensional wavenumber and frequency spectrum; but because of the complexity of the subject, this latter point will be described elsewhere.

The basic data used here are the current meter mooring observations accumulated from a variety of sources over the past two decades. The data prove only marginally suitable to our goal, and the results can be regarded as, at best, a semiqualitative first estimate, which will surely be revised in the future. Nonetheless, it seems to be a useful starting point, if only to provide a convenient target for readers, and which will perhaps stimulate the necessary observations. The altimetric data will be taken up following the discussion of the current meters. A better method for deducing the vertical partitioning, which will become available as numerical circulation models improve, will be discussed at the end.

Corresponding author address: Dr. Carl Wunsch, Dept. of Earth, Atmospheric and Planetary Sciences, Massachusetts Institute of Technology, Cambridge, MA 02139-4307.
E-mail: cwunsch@pond.mit.edu

2. The data and methods

The questions posed are specifically: 1) What is the partition throughout of the water column of the kinetic energy of time-varying motions amongst the dynamical modes? 2) What is the partition of the surface kinetic energy amongst the dynamical modes? The implied question is: Given the surface geostrophic velocity as measured by an altimeter, how is the motion to be interpreted as a function of depth? (Although we will not continue to call attention to it, results here are confined to the time-varying elements of the general circulation.)

Two representations have been commonly used in the past: 1) dynamical modes and 2) empirical orthogonal functions (EOFs), and we discuss these separately.

a. Linear dynamical modes

The approach can be understood through a specific example. Figure 1 depicts the horizontal velocity normal modes of a flat-bottom linear ocean satisfying the equation

$$\frac{d}{dz}\left(\frac{1}{N^2(z)}\frac{dF}{dz}\right) + \gamma^2 F(z) = 0, \qquad (1)$$

where $N(z)$ is the buoyancy frequency, subject to rigid upper and lower boundary conditions (see, e.g., Gill 1982 or Wunsch and Stammer 1997), whose solutions are the modes $F_n(z)$, γ_n, $0 \le n \le \infty$, γ_n being an eigenvalue. The zeroth mode is rigorously, in this context, the barotropic one. Here $N(z)$ was computed at each mooring position from the annual mean climatology of Levitus and Boyer (1994). Picaut and Sombardier (1993) discuss the accuracy of mode computation in the tropical Pacific. Their conclusion that the density field in the upper 600 m of the water column is most important in the computation is consistent with the experience here and is fortunate owing to the paucity of reliable deep values in the climatology. Superimposed upon the modes in the figure are the depths, z_i, of current meters from an experiment at (47.4°N, 20°W) discussed by Arhan et al. (1989). The current meter records, filtered to a once per day value, are denoted $u_i(z, t)$, $v_i(z, t)$. The basic assumption is that

$$u_i(t) = u(z_i, t) = \sum_{n=0}^{N} \alpha_{un}(t) F_n(z_i) + n_{ui}(t), \quad 1 \le i \le M, \; 1 \le t \le L \qquad (2)$$

$$v_i(t) = v(z_i, t) = \sum_{n=0}^{N} \alpha_{vn}(t) F_n(z_i) + n_{vn}(t), \quad 1 \le i \le M, \; 1 \le t \le L, \qquad (3)$$

where n_{ui}, n_{vi} are noise residuals and N is the number of modes fit [not to be confused with the buoyancy frequency, $N(z)$].

There are a number of problems. The modes F_n are directly applicable for a (i) linear, (ii) resting ocean with a (iii) flat bottom. All three of these assumptions are false to some extent almost everywhere. The central justification for nonetheless using the F_n as representational basis functions are that Sturm–Liouville theorems applied to (1) show that they are a complete set and that in practice at a great many locations a very small number of low modes suffices to reproduce the data with high accuracy. A referee has asked about using modes based upon the presence of intensified near-surface flows $U(z)$. This possibility will be discussed at the end. Here we remark only that the weakest part of the analysis concerns the few available data, not the mode shapes.

b. The database

Records were obtained from a number of sources, listed in the acknowledgments, but the compilation here is inevitably incomplete, representing a somewhat arbitrary decision to stop with the understanding that in the future, analysis of a more complete dataset may be justified. It is an oddity of modern oceanography that the duration of the comparatively exotic TOPEX/POSEIDON altimeter mission (four years at the time of writing) already exceeds the duration of all but a handful of conventional current meter moorings. Most of the exceptions are in the eastern Atlantic data described by Müller and Siedler (1992) and there are a few two- and three-year mooring deployments in the western North Pacific and North Atlantic. The results obtained here strongly suggest that a minimum of three years of record is required for even marginal statistical stability with much longer requirements in some areas (discussed further below).

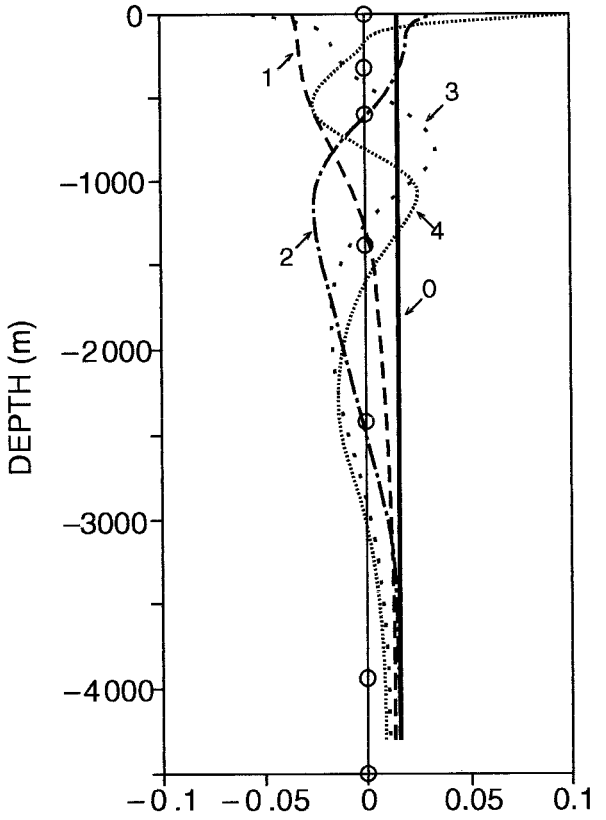

FIG. 1. Horizontal velocity modes 0 to 4 from near 47.4°N, 20°W (mooring 59). An important point is the surface intensification of the baroclinic modes, including the first one.

For the analysis, it is strongly preferred for modal fitting that instruments at least straddle the main thermocline; lie in water of at least 4000 m; have an instrument within 100 m of the surface; have six or more instruments; and have a duration exceeding two years. The set of moorings fulfilling this prescription is empty, and in practice, all but the thermocline-straddling and depth requirements had to be relaxed to obtain useful geographical coverage (and some compromises were made with the depth requirement as well). Table 1 lists the moorings that were used in the final analysis and Fig. 2 shows their locations. A reference, where known, permitting a reader to find published discussion of the individual moorings by the original PIs is listed in the table (if the moorings were discussed in several papers, the latest one known is used).

TABLE 1. Basic information about moorings analyzed, which are generally sorted by longitude within each ocean basin (North Pacific, North Atlantic, South Atlantic, Indian Oceans). For each mooring there is an arbitrary designation number, latitude, longitude, duration in days (D), number of instruments (M), the water depth (h) in meters, and the equivalent depth (h_1) in centimeters. The latter can readily be converted to the first baroclinic Rossby radius of deformation as $r_1 = \sqrt{gh_1}/f$ where f is the local Coriolis parameter. Then for each mooring the successive columns are ⟨ke⟩: the vertical average kinetic energy/unit mass (cm^2 s^2); ⟨e-ke⟩: the estimated error in the vertical average kinetic energy; ''ratio,'' the ratio $T^{(2)}(0)/T^{(1)}(0)$ of surface kinetic energy in the modal sum to that assuming phase-locking; the percentage of the mean kinetic energy in the barotropic and first baroclinic modes of the u component of $T^{(2)}(0)$; the percentages in the v component; the percentages of surface kinetic energy $T^{(2)}(0)$ for the two components in the barotropic and first baroclinic modes (labeled $\%uF_1$, $\%uF_1$, etc.) and the subjective weight w_i; and the objective weight W_i. The final column is the most recent reference known to the author that leads to a discussion of the particular mooring.

Data from the last seven moorings listed were obtained after this paper was written and, although tabulated here, are not discussed in the text. They include moorings from south of the Circumpolar Current, on the equator in the Indian Ocean, and one additional western Pacific mooring (see Fig. 2).

A much more complete listing of results is available from the author.

#	Lat	Long	D	M	h	h_1	⟨ke⟩	⟨e-ke⟩	ratio	$\%u_0$	$\%u_1$	$\%v_0$	$\%v_1$	$\%uF_0$	$\%uF_1$	$\%vF_0$	$\%vF_1$	w_i	W_i	Reference/PI
12	27.9	151.9	373	5	6057	118	50	1	0.82	16	28	10	36	1	17	1	21	0.80	2.47	Niiler and Hall 1988
14	28.0	151.9	298	5	6078	118	53	1	1.19	16	27	11	35	2	27	1	33	0.80	1.58	Schmitz 1988
13	34.9	152.0	372	5	6158	94	141	1	0.42	45	34	55	31	7	55	10	59	0.90	2.50	*
15	32.5	152.1	307	4	5728	109	63	16	0.38	49	39	27	59	10	71	4	79	1.00	1.01	*
16	32.5	152.1	373	4	5756	109	295	21	4.52	6	28	6	26	1	23	1	21	0.30	1.50	*
28	31.0	164.9	391	3	6079	70	13	20	0.35	32	45	29	52	5	56	5	64	1.00	0.98	*
29	39.0	165.0	383	3	5317	77	19	32	0.45	20	66	17	67	3	78	2	77	1.00	0.82	*
26	33.0	165.0	692	3	6262	104	43	50	0.52	26	66	51	42	3	87	9	79	1.00	3.17	*
30	41.1	165.0	380	3	5350	77	4	5	0.57	30	59	40	46	4	78	7	69	1.00	0.82	*
95	37.0	165.0	384	3	5098	76	31	49	0.51	19	73	17	74	3	87	2	85	1.00	0.79	*
4	34.3	167.0	348	3	5730	88	15	13	1.37	52	45	51	45	11	80	11	80	1.00	0.73	Hamann and Taft 1987
5	39.0	171.1	273	3	6150	76	3	3	31.61	74	10	61	19	27	26	16	39	0.01	0.48	*
23	39.0	175.0	373	3	4926	70	9	14	0.52	34	52	32	59	6	68	6	78	1.00	0.72	Schmitz 1988
22	31.0	-175.1	709	3	5431	84	12	15	0.53	23	68	32	56	3	83	5	75	1.00	2.88	*
25	35.1	-175.0	712	3	5650	25	14	19	0.53	20	73	22	66	3	87	3	81	1.00	3.02	*
27	41.0	-175.0	717	3	5795	25	3	4	0.41	26	57	46	35	4	70	9	54	1.00	3.14	*
24	39.0	-174.9	716	3	5821	18	7	11	0.44	22	64	22	61	3	77	3	72	1.00	3.15	*
20	35.0	-152.0	704	3	5733	1	1	1	0.57	41	42	40	49	7	62	6	73	1.00	3.00	*
21	39.0	-152.0	704	3	6125	2	2	2	0.54	32	51	24	55	4	64	3	62	1.00	3.20	*
44	0.3	-144.5	375	6	4300	2	174	19	0.51	5	50	6	40	0	57	1	61	1.00	2.55	Eriksen 1985
51	32.7	-128.1	388	4	4524	2	3	5	0.57	35	51	43	39	5	77	6	65	1.00	1.28	Brink 1995
3	39.5	-127.7	346	6	5730	2	14	0	0.34	42	29	38	28	7	54	6	50	0.70	2.90	Pillsbury et al. 1985
8	38.2	-124.4	285	5	3757	1	10	0	0.42	19	28	23	47	2	30	3	55	1.00	0.89	R. L. Smith
35	34.0	-70.0	381	6	5366	71	114	1	0.35	59	24	37	40	12	39	5	45	1.00	3.29	Lippert and Briscoe 1990
31	34.0	-70.0	335	10	5366	89	48	0	1.50	61	34	61	30	15	70	15	60	0.80	7.06	*
61	38.8	-68.1	807	4	3810	48	39	139	5.93	35	56	30	60	5	76	4	75	0.10	4.66	Shay et al. 1995
63	38.3	-68.0	353	3	4275	54	51	58	3.12	57	30	58	31	10	54	11	57	0.80	0.56	*
62	37.3	-67.6	343	4	4821	64	394	195	1.80	38	42	60	28	5	49	11	49	1.00	1.06	*
60	36.8	-67.5	651	4	4975	69	342	123	0.79	55	31	62	23	10	48	12	38	0.80	3.96	*
52	23.2	-64.0	402	4	5847	98	8	6	27.01	68	13	66	14	13	28	12	28	1.00	1.77	Pillsbury et al. 1985
53	23.2	-64.0	327	4	5835	98	5	4	40.94	56	22	68	18	9	40	14	42	0.60	1.17	*
2	23.3	-64.0	346	4	5846	98	14	4	60.69	44	36	45	36	6	57	6	60	1.00	1.31	*
6	40.5	-62.0	507	4	4886	50	100	45	12.42	60	9	37	19	12	17	5	26	1.00	2.36	Hogg et al. 1986
36	34.0	-60.0	232	4	4687	93	32	14	2.38	57	34	27	67	14	60	4	77	0.80	0.47	Schmitz and Luyten 1991
92	39.0	-59.0	358	3	5140	60	214	156	2.65	78	19	74	23	26	57	22	61	1.00	0.70	*
90	39.5	-59.0	278	4	5167	60	232	106	1.70	75	22	74	23	23	60	21	63	0.95	0.75	*
38	35.6	-55.1	219	4	5162	91	105	35	5.95	80	17	70	26	29	47	20	59	0.90	0.46	*
37	35.9	-55.1	224	4	5167	86	106	37	4.36	67	30	78	19	20	63	30	53	0.90	0.49	*
39	34.9	-55.0	219	4	5515	93	74	24	5.25	86	11	67	29	39	37	19	64	0.90	0.50	*
41	37.5	-55.0	304	4	5310	83	119	41	3.60	68	28	85	13	19	63	37	47	0.90	0.92	*
42	31.6	-54.9	243	7	5595	95	16	3	0.83	36	49	33	54	6	64	5	69	0.95	1.90	*
40	35.9	-54.7	235	4	5318	90	105	34	3.80	91	7	73	22	50	29	23	55	0.90	0.55	*
57	40.1	-54.7	436	4	5193	59	250	102	3.00	85	12	89	9	33	47	41	41	1.00	1.85	Bower and Hogg 1996
58	40.9	-54.7	701	5	5062	50	162	0	0.30	72	22	56	34	18	52	10	56	1.00	7.29	*
43	16.7	-54.3	355	4	5000	78	118	3	0.56	54	22	36	13	7	40	4	21	1.00	1.18	Fu et al. 1982
46	15.0	-54.2	350	5	5300	79	9	0	0.64	36	28	43	26	3	36	4	37	1.00	1.90	*
45	15.2	-53.2	353	4	5300	79	14	4	2.39	48	17	26	15	5	24	2	15	1.00	1.24	*
91	57.0	-51.6	207	4	3560	9	62	17	208.98	57	14	49	19	9	7	7	9	0.80	0.29	*
48	28.0	-48.1	339	3	4800	84	8	9	0.58	29	62	31	62	5	82	5	84	1.00	0.58	*
34	38.9	-46.9	383	3	5332	71	103	60	2.65	72	25	68	28	23	65	20	68	1.00	0.83	Fofonoff and Hendry 1985
94	43.2	-46.7	520	4	3987	34	43	33	0.99	73	14	65	21	21	29	16	37	1.00	2.02	*
93	44.4	-45.7	534	3	4023	32	42	57	1.05	77	9	71	9	26	20	21	19	0.90	1.21	*
89	51.1	-44.6	259	3	4059	16	106	128	2.31	75	17	78	13	23	41	24	31	0.40	0.29	A. Clarke 1996 personal communication

The chief difficulty is that of duration. Figure 3 is not an untypical midocean record, from the north-central Pacific Ocean. One sees visually, what is confirmed by a spectral analysis, that most of the energy lies in low-frequency components (the spectrum is quite ''red'') and that the second year is visually different in character from the first one. As far as the energy dominant components are concerned, there are too few degrees of freedom available to make any statistically significant inferences. Even a full year of data is much too

TABLE 1. (*Continued.*)

#	Lat	Long	D	M	h	h_1	<ke>	<e-ke>	ratio	$\%u_0$	$\%u_1$	$\%v_0$	$\%v_1$	$\%uF_0$	$\%uF_1$	$\%vF_0$	$\%vF_1$	w_l	W_l	Reference/PI
32	39.0	-44.1	388	5	4960	74	65	28	6.26	37	22	43	27	5	21	6	29	0.30	2.19	Fofonoff and Hendry 1985
9	39.0	-44.1	166	6	4960	84	44	22	6.25	60	27	38	32	13	60	6	51	1.00	0.58	*
7	39.6	-42.1	212	4	4995	65	48	17	1.28	32	62	50	45	6	86	12	78	1.00	0.42	*
33	39.0	-42.0	396	3	4788	74	13	9	2.44	62	31	37	58	18	65	7	81	0.90	0.79	*
47	27.2	-40.4	346	3	4800	79	10	13	0.56	29	62	23	67	5	80	4	82	1.00	0.61	*
56	48.0	-34.0	344	4	4300	39	58	35	0.44	28	64	33	61	5	79	6	80	1.00	0.95	Colin de Verdiere et al.1989
85	21.9	-25.2	277	4	5143	73	6	3	0.36	28	46	41	36	3	49	6	45	0.95	0.74	*
17	31.5	-24.7	217	3	5444	79	8	8	0.44	45	46	54	40	10	76	14	74	1.00	0.27	from IOS Wormley
87	20.4	-24.4	252	4	4700	68	6	2	0.56	41	34	47	27	6	40	7	32	0.90	0.56	Mueller and Siedler 1992
88	20.4	-24.4	278	4	4694	68	3	1	1.12	36	30	45	28	4	31	6	33	0.80	0.68	*
86	21.2	-24.4	278	5	4960	68	4	0	0.73	49	22	47	31	7	28	8	42	0.90	1.12	*
72	20.5	-23.6	254	4	4580	63	7	3	1.18	21	42	39	38	2	36	6	43	1.00	0.55	*
83	20.4	-23.6	210	5	4540	63	5	0	0.43	17	46	27	33	2	40	3	30	1.00	0.59	*
84	20.4	-23.6	277	5	4500	63	7	0	0.49	25	24	27	38	3	20	3	36	1.00	1.01	*
10	30.3	-23.4	256	5	5296	80	5	2	0.42	59	9	53	22	14	16	12	37	0.50	1.02	MAFF Lowestoft
18	41.7	-22.0	372	4	3840	50	11	3	6.64	24	14	24	10	4	13	4	8	0.30	1.00	*
80	33.1	-22.0	300	5	5285	76	4	0	1.69	45	17	40	24	8	22	7	28	0.90	1.39	Mueller and Siedler 1992
79	33.1	-21.9	364	4	5276	76	4	2	21.87	73	13	34	46	22	29	6	56	0.95	1.31	*
77	33.2	-21.9	306	6	5290	76	19	1	0.40	18	32	27	44	2	32	4	50	0.80	2.09	*
82	33.1	-21.9	280	5	5190	76	7	1	0.37	56	26	32	53	13	44	5	65	1.00	1.19	*
75	33.2	-21.9	237	5	5290	76	18	5	1.68	30	37	34	24	4	39	1	30	0.20	0.87	*
81	33.1	-21.9	280	7	5281	76	4	0	0.53	39	32	52	27	6	39	11	40	0.90	2.38	*
78	33.1	-21.9	317	7	5285	76	5	0	0.51	44	33	48	36	8	44	10	52	0.90	3.05	*
76	33.2	-21.8	277	6	5295	76	36	5	1.24	58	23	48	32	14	42	10	49	0.30	1.72	*
59	47.4	-20.6	403	5	4492	51	38	0	0.42	42	49	39	51	10	63	9	63	1.00	2.14	Colin de Verdiere et al. 1989
74	22.9	-20.5	355	5	4146	60	18	0	0.28	9	41	8	39	1	32	0	29	1.00	1.53	Mueller and Siedler 1992
73	26.0	-18.0	323	5	3430	54	15	0	0.36	28	46	33	45	6	49	7	53	1.00	1.05	*
19	52.5	-17.7	370	4	4135	39	145	27	1.75	44	15	47	17	12	22	13	25	0.20	1.06	Gould 1983
50	47.0	-14.8	239	8	4300	56	12	2	0.59	27	68	45	51	8	87	15	79	0.90	1.84	Colin de Verdiere et al. 1989
11	47.3	-10.0	347	5	4395	54	8	0	0.48	39	46	43	44	14	69	16	67	1.00	1.55	MAFF Lowestof
70	-30.1	-41.7	695	4	3814	71	21	6	19.48	50	16	54	15	9	17	10	17	0.40	3.46	Hogg et al. 1996
1	-48.1	-41.3	277	5	5889	48	662	36	0.24	29	24	30	26	4	17	5	19	1.00	1.32	Whitworth et al 1991
71	-31.2	-39.8	566	4	3920	70	33	7	6.00	23	31	52	15	3	25	10	16	0.30	2.36	Hogg et al. 1996
69	-31.1	-39.4	683	7	4675	76	299	1	1.49	22	5	23	1	3	4	3	1	0.30	12.53	*
55	-30.0	6.0	493	4	5180	78	48	17	0.60	60	24	54	30	15	47	12	54	0.70	2.36	Garzoli et al. 1996
54	-30.0	8.8	494	3	5003	72	34	52	0.61	40	46	39	40	8	68	7	57	0.80	1.29	*
64	-38.0	15.5	720	3	4831	57	153	159	19.19	78	12	74	12	21	34	18	31	0.95	2.64	Luyten et al. 1990
67	-42.0	17.8	637	3	4831	56	54	54	0.33	59	33	45	45	17	62	10	67	0.95	2.07	*
68	-38.0	18.5	704	4	4705	71	319	77	3.72	75	22	65	32	27	61	19	70	0.90	4.38	*
66	-37.2	23.0	612	4	5318	90	96	81	0.72	45	44	52	35	10	62	13	53	1.00	3.74	*
65	-35.9	27.0	684	4	4649	90	97	28	0.65	40	52	36	54	10	73	9	71	1.00	4.08	*
49	-0.4	58.0	390	4	4800	82	1	0	1.83	21	18	17	21	2	26	1	25	0.60	1.37	Luyten et al. 1980
97	-64.5	-45.9	376	4	4420	8	4	1	0.78	46	24	54	22	5	31	7	35	0.95	1.17	E. Fahrbach 1996 personal communication
98	-66.6	-27.1	401	4	4830	8	662	36	1.19	70	17	63	17	10	17	6	12	0.90	1.46	*
100	2.2	80.5	411	5	4490	80	14	0	0.64	23	17	23	15	18	22	19	20	0.70	2.22	F. Schott 1996 personal communcation
101	4.6	80.5		6	4382	81	15	13	1.85	34	12	35	19	4	21	4	35	0.70	3.14	*
96	5.0	80.5	419	7	4295	82	416	1	0.49	10	24	9	24	1	26	1	27	0.90	4.33	*
102	5.0	80.6		6	4329	82	3	3	89.10	16	16	15	19	1	22	1	28	0.50	2.61	*
99	35.6	142.7	332	4	6380	92	14	4	3.05	30	47	25	41	3	54	2	44	0.80	1.32	Z. Hallock 1996 personal communcation

short to characterize the variability seen: for example, Schmitz (1989), Müller and Siedler (1992), and the results reported here.

Because of the database problem, the results will have only some rough validity based upon averaging horizontally over large areas and many deployment years. For completeness, analyses for a number of moorings substantially deviating from the nominal requirement (typically those of duration short compared to a year) are included here, but were downweighted in the mapping of the results.

3. Linear mode fits

a. Basic results

Because the available data are so inhomogeneous in vertical and temporal coverage, and generally marginal for the purpose to which we are putting them, the methodology employed for modal fitting was based upon an a priori statistical hypothesis, with the data used to test, and hence accept or reject that hypothesis. From inferences from the existing literature (McWilliams 1976; Richman et al. 1977; Müller and Siedler 1992; Fu et al. 1982; Mercier and Colin de Verdiere 1985; and others) it was assumed a priori that the vertical partitioning of the kinetic energy of the linear modes was in the ratio 1:1:1/2:1/4:1/8 for the barotropic through fourth baroclinic modes. That is, equipartition was assumed for the horizontal kinetic energies of the barotropic and first baroclinic modes. The modal coefficients were then calculated from the data using the Gauss–Markov estimate

$$\bar{\boldsymbol{\alpha}}_u(t) = \mathbf{P}_u(0)\mathbf{A}^{\mathrm{T}}(\mathbf{A}\mathbf{P}_u(0)\mathbf{A}^{\mathrm{T}} + \sigma_n^2\mathbf{I})^{-1}\mathbf{U}(t), \qquad (4)$$

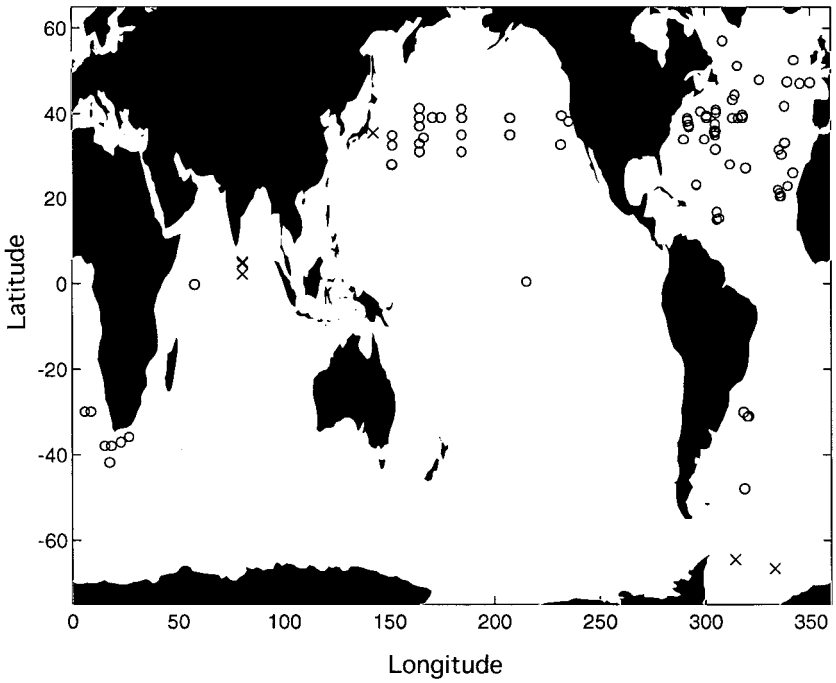

FIG. 2. Positions of the moorings (open circles) analyzed in this paper and listed in Table 1. Data from positions labeled "×" arrived after this paper was written and are listed in Table 1, but are not otherwise discussed.

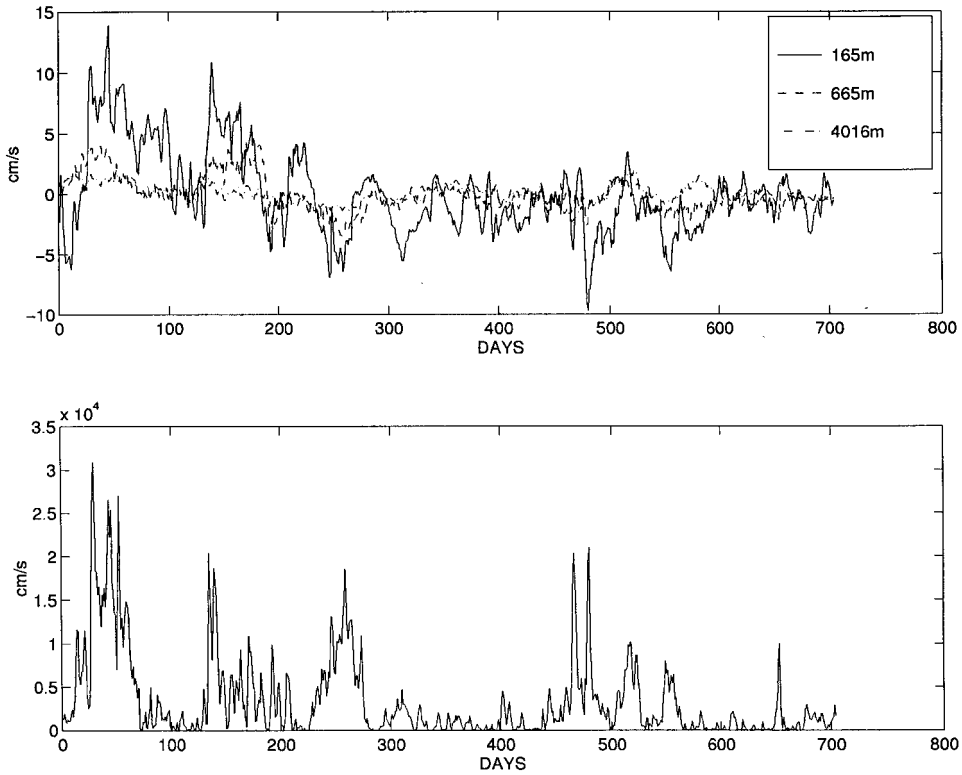

FIG. 3. (Upper panel) Zonal component of velocity (all energy at periods shorter than about one day having been removed) from the central Pacific Ocean at 35°N, 152°W (mooring No. 13). (Lower panel) Squared amplitude of the barotropic mode from the record in the upper panel. Energetic events at the beginning of the first year are not obviously present at the end of the second year.

(Liebelt 1967; Wunsch 1996) thus producing a minimum variance estimate subject to the prior statistics. Here $\mathbf{U}(t)$ is the matrix whose columns j are the $u_j(t)$ with time means removed, filtered to remove all energy at periods shorter than about one cycle per day; σ_n^2 is an estimate of the observational noise of current meters, and $\mathbf{P}_u$ (0) is a diagonal matrix representing the a priori energy,

$$\mathbf{P}_u(0) = \langle \bar{\boldsymbol{\alpha}}_u(t)\bar{\boldsymbol{\alpha}}_u(t)^{\mathrm{T}}\rangle \equiv E_u^2 \mathrm{diag}([1\ 1\ 1/2\ 1/4\ 1/8])/2.88, \quad (5)$$

where E_u^2 is an estimate of the total energy in the records, calculated from $\mathbf{U}$ itself, and 2.88 is the sum of the a priori weights. Matrix $\mathbf{A}$ is defined as

$$\mathbf{A} = M \updownarrow \{\underbrace{F_0(z_i)\ F_1(z_i)\ \cdots F_4(z_i)}_{5}\},$$

and diag (**x**) is the diagonal matrix with values **x**. The uncertainty of the estimates was then calculated as

$$\mathbf{P}_u(1) = \langle (\bar{\boldsymbol{\alpha}}_u(t) - \boldsymbol{\alpha}_u(t))(\bar{\boldsymbol{\alpha}}_u(t) - \boldsymbol{\alpha}_u(t))^{\mathrm{T}}\rangle = \mathbf{P}_u(0) - \mathbf{P}_u(0)\mathbf{A}^{\mathrm{T}}(\mathbf{A}\mathbf{P}_u(0)\mathbf{A}^{\mathrm{T}} + \sigma_n^2\mathbf{I})^{-1}\mathbf{A}\mathbf{P}_u(0), \quad (6)$$

the standard expression for a Gauss–Markov estimate. Similar expressions were used for $\bar{\boldsymbol{\alpha}}_v$, which is calculated independently. Here σ_n^2 was taken uniformly as equivalent to an rms error of 0.3 cm s^{-1}. A more rigorous analysis based upon detailed computations with each mooring would produce σ_n^2 values varying from location to location and with depth and frequency. In practice, the results are generally insensitive to considerable variations in σ_n^2, and given the belief that the chief uncertainties arise from the short record durations and not from intrinsic error, the uniform value was adopted to minimize the analysis effort.

A number of experiments were carried out on a number of moorings using varying numbers of modes and weights, including, especially, three-mode fits. Although there are many detailed differences in the results compared with five-mode fits with the present weights, the results remained qualitatively similar. Ultimately, it was concluded that retaining a uniform procedure rendered the method and interpretation more transparent than did a variable procedure. Experiments with output from a general circulation model—to be reported elsewhere—in which overdetermination of the least squares system was easy, produced modal decompositions over much of the ocean much like those found here. Overdetermination renders the solutions independent of the a priori hypothesis.

We are interested not in $\bar{\boldsymbol{\alpha}}_u(t)$, $\bar{\boldsymbol{\alpha}}_v(t)$ but in their sample mean squares over the record; that is,

$$\langle \tilde{\alpha}_{ui}(t)^2\rangle_L \equiv \frac{1}{L}\sum_{t=1}^{L} \tilde{\alpha}_{ui}(t)^2, \quad (7)$$

etc. and their uncertainty (a covariance). The strong autocorrelation evident in Fig. 3a translates into a strong autocorrelation in the estimates of $(\bar{\boldsymbol{\alpha}}_u(t))^2$ (see Fig. 3b), and the uncertainty calculation for (7) cannot treat the L estimates as independent. To obtain an estimate of the uncertainties of the mean-square values of $\tilde{\alpha}_{ui}(t)^2$, $\tilde{\alpha}_{vi}(t)^2$, it was assumed that the $\bar{\alpha}_{ui}(t)$ were zero-mean Gaussian random variates, with a sample autocovariance $\tilde{R}(\tau)$. Equation (5.3.28) of Priestley (1981),

$$\langle (\tilde{R}(0) - R(0))^2\rangle \approx \frac{2}{L}\sum_{m=-\infty}^{\infty} R^2(m), \quad (8)$$

is used to calculate the uncertainty of the mean squares, with the covariance of the fourth moments of Gaussian random variates $\mathbf{P}_u^{(2)}$, $\mathbf{P}_v^{(2)}$ taken from Kotz and Johnson (1985). The true value of $R(m)$ in (8) is unknown, and the sum was simply taken to be that computed from the sum over the sample autocovariance of α_{u1} of the result from a Nares Abyssal Plane mooring. These estimates produced a ratio

$$\sum_{m=-\infty}^{\infty} \frac{\tilde{R}^2(m)}{L} = \frac{1}{6.2};$$

that is, suggesting about six degrees of freedom from one year of record. Although there is some variability in this number, it was kept fixed to produce a simple rough estimate of the uncertainties. (The decorrelation timescales for all modes on all moorings were computed and would permit the reader to calculate an improved uncertainty estimate for each value should that be desired.)

An advantage of this estimation method, in addition to its ability to exploit prior information, is that the expressions are useful (up to the validity of the prior information) for an arbitrary number of instruments. In practice, data from three instruments were often used to infer the coefficients for five modes—a perfectly reasonable procedure, which essentially becomes a test of the five-mode hypothesis. (Data from three instruments cannot prove the hypothesis of the validity of the a priori variance distribution; they can however disprove it, and some examples are described later.) Even for moorings where, on average, the modal fit does a good job of representation, the results are sometimes not uniformly accurate over the record. Figure 4 shows the breakdown of the modal fit during isolated events occurring during the data duration.

Partial results from this procedure are displayed in Table 1. For each mooring the estimated percentage of the water column average kinetic energy found in the first barotropic and first baroclinic modes for u, v separately are listed. Confidence limits on the results are taken up below.

1) KINETIC ENERGY

The results permit us to estimate the water column average kinetic energy as

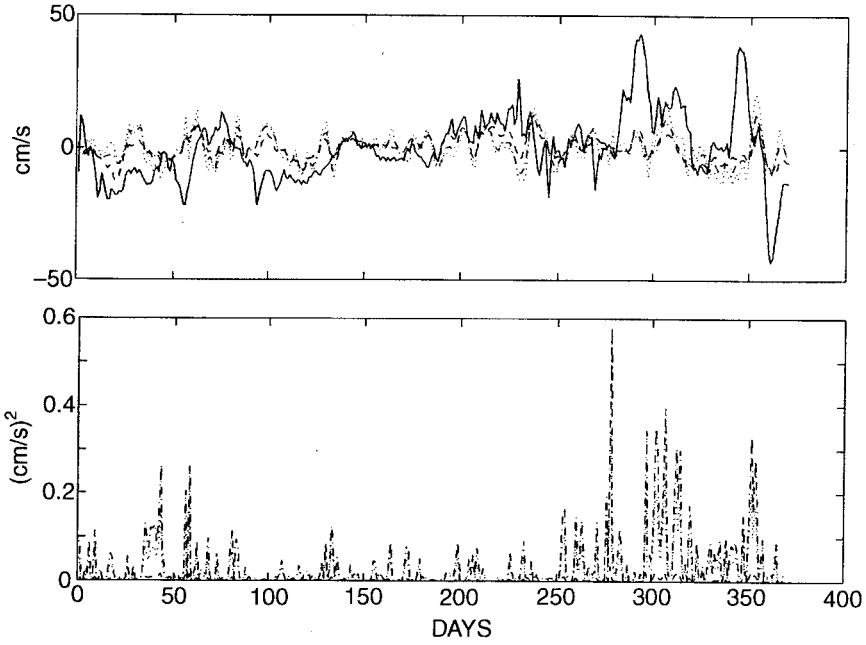

FIG. 4. Zonal component of filtered flow at a mooring located at 52.5°N, 17.7°W (upper panel), and the residuals (lower panel) through time from a five-mode fit. Bursts of energy in the latter suggest a nonuniformity of the modal hypothesis through time, but the overall fit was deemed adequate.

$$T_h = \frac{1}{h}\int_{-h}^{0}\frac{1}{2}(u^2 + v^2)\,dz$$

$$= \frac{1}{2h}\sum_{n=0}^{4}(\langle\tilde{\alpha}_{un}(t)^2\rangle_L + \langle\tilde{\alpha}_{vn}(t)^2\rangle_L). \qquad (9)$$

The result, Eq. (9), depends upon the orthonormality of the $F_n(z)$ with the normalization used giving each a vertical mean-square integral of unity, and the orthogonality rendering the result independent of correlations $\langle\alpha_{ui}\alpha_{uj}\rangle \neq 0$, etc. The units in Table 1 are cm^2 s^{-2} with the water density $\rho = 1$, and the square root of the estimated variance is listed. These vertical average estimates are a complement to Dickson's (1989) compilation of point values for individual current meters.

2) SURFACE KINETIC ENERGY

For comparison with altimetry, we require an estimate both of the total *surface* kinetic energy and the fraction in each mode, but actually doing so raises the question of the temporal orthogonality of the modes. Consider that, for example, the kinetic energy at any fixed level, z_i (including the special case $z_i = 0$),

$$T^{(1)}(z_i) = \frac{1}{2L}\sum_{t=1}^{L}\left\{\left(\sum_{n=0}^{N}\tilde{\alpha}_{un}(t)F_n(z_i)\right)^2 + \left(\sum_{n=0}^{N}\alpha_{vn}(t)F_n(z_i)\right)^2\right\} \qquad (10)$$

reduces to

$$T^{(2)}(z_i) = \frac{1}{2L}\sum_{t=1}^{L}\left(\sum_{n=0}^{N}\tilde{\alpha}_{un}(t)^2F_n(z_i)^2 + \sum_{n=0}^{N}\tilde{\alpha}_{vn}(t)^2F_i(z_i)^2\right), \qquad (11)$$

the sum over the squared modal coefficients, only if $\langle\alpha_{un}\alpha_{un'}\rangle = 0$, $n \neq n'$, etc. That is, if to the contrary, the sample coefficients are correlated in time, the kinetic energy is not the sum of the kinetic energies in the individual modes. [Equation (9) for the total kinetic energy is rendered correct by the *vertical* orthogonality of the modes.] The surface kinetic energy was therefore computed according to both formulas (10) and (11), and the ratio of the two becomes a rough integral measure of the degree of modal correlation found in the mooring (Table 1). The spatial distribution of the phase locking is described further under "problematic results."

But, it is only $T^{(2)}$ that permits us to speak of the fraction of the kinetic energy in each mode at the sea surface. These are expressed as percentages of the total surface kinetic energy $T^{(2)}(0)$ in Table 1. Fortunately, with some notable exceptions described later, $T^{(1)}(0)$, $T^{(2)}(0)$ are generally within a factor of 2–3 almost everywhere, with the pattern of spatial variability in the two definitions being very similar. Computation of the total surface kinetic energy is, however, problematic. On most moorings, the uppermost current meter is typically several hundred meters from the surface and the surface intensification visible in most of the baroclinic

modes implies that the extrapolation to the surface is intrinsically unstable. For moorings with strong modal correlations, we see both surface intensification and surface cancellation owing to the phase coupling.

3) THE FIT RESULTS

One can anticipate, a priori, the possibility of the dependence of the vertical partition on a large number of physical parameters, including possibly, latitude, water depth, topographic roughness on different spatial scales, duration, kinetic energy of the variability, proximity to eastern and western boundaries, mean vertical and/or horizontal shear, stratification, etc. Furthermore, a frequency domain analysis (discussed below) shows that the partition is a function of frequency.

Although some specific symptomatic problems will be briefly described below, a discussion of the result of each mooring is too voluminous. But each mooring is in some way unique. A full spreadsheet (about 200 columns for each mooring) of detailed numerical results is available directly from the author.

A major part of our results is based upon spatial maps of the aggregated results. The uncertainty of the kinetic energy listed for each mooring is one simple measure of the reliability of the individual results. But because there are many elements to the reliability of the modal decomposition a weight was computed for the results from each mooring. The weight for mooring i was defined as the product of

$$W_i = \left(\frac{D}{365}\right)^2 \left(\frac{M}{4}\right)^2 \left(\frac{h}{4000}\right), \quad \text{and } w_i, \qquad (12)$$

where D is duration in days, h is the water depth in meters, and M is the number of instruments, thus giving greatest weight to long records in deep water with multiple instruments on the mooring. However, W_i does not account for all difficulties, for example, a maldistribution of instruments in the vertical and a poor fit for any of a number of reasons. Thus, w_i is a subjective scale factor, which is normally unity, but is sometimes quite small when a decision is made to downweight the result. At the outset of this study, it was unclear whether any useful result would emerge from the potentially very large number of parameters affecting the vertical current stretch-out, and the data availability appears at best marginal. It is rare that *any individual mooring gives statistically significant results*; rather, it is only the emergence of stable spatial patterns from the aggregate of large numbers of moorings, as a space and time average over large distances and over all times of measurement that lends substance to the results.

4) OVERALL RESULTS

We will summarize the results for the three basins, the North and South Atlantic and the North Pacific, where there is some approximation to large-scale coverage. The South Atlantic coverage is on the edge of practical utility, and the North Pacific results are confined to a narrow latitude band between about 25° and 35°N.

For each basin, we display in the figures maps of the logarithm of the kinetic energy per unit depth and of the approximate percentage of the kinetic energy found in the barotropic and first two baroclinic modes. We also display the logarithm of the estimated surface kinetic energy and the percentage found in the barotropic and first two baroclinic modes under the assumption of modal noncorrelation. Because of the general surface intensification of the baroclinic modes, the partition of modal energy is different (usually higher in the baroclinic modes) at the surface than it is for the water column average.

These maps were objectively drawn, but are not optimal. A simple interpolation scheme was chosen to reflect a subjective judgement as to plausible contouring. The weighting given to each mooring was that in Eq. (12).

5) THE TOTAL KINETIC ENERGY

In the North Pacific and Atlantic, Figs. 5a and 7a show the expected westward intensification into the western boundary current regions. As with all the properties, the spatial coverage within the boundary current regimes themselves is inadequate to produce confidence that the property extremes have actually been found, and the mapping procedure tends to average values lying in different dynamical regimes. The extremes of mean vertical kinetic energy per unit mass range from about 660 $cm^2\ s^{-2}$ at the edge of the Falkland Plateau (Whitworth et al. 1991) to a minimum of about 1.4 $cm^2\ s^{-2}$ near 210°E, 25°N in the eastern Pacific. The maximum in the two Northern Hemisphere basins are both near 310 $cm^2\ s^{-2}$ in the Kuroshio and Gulf Stream. To the extent that the surface kinetic energies reflect the water column values, the TOPEX/POSEIDON data (see Wunsch and Stammer 1995; Stammer 1997) suggest that none of the moorings was placed in the quietest parts of the oceans, which appear to be in the northeast Pacific and (unexpectedly) in parts of the Southern Ocean. [In elevation slope, i.e., without the effects of increased Coriolis parameter (not shown), the quietest areas are in the eastern South Atlantic and Pacific near 20°S.]

6) MODAL DECOMPOSITION OF TOTAL KINETIC ENERGY

The North Pacific kinetic energy is, crudely speaking and up to the spatial sampling limitations, about 35% contained in the barotropic mode and about 55% in the first baroclinic mode with the latter reaching peaks near 70% around 180° longitude. In contrast, the North Atlantic, which is better sampled, is on average about 40%

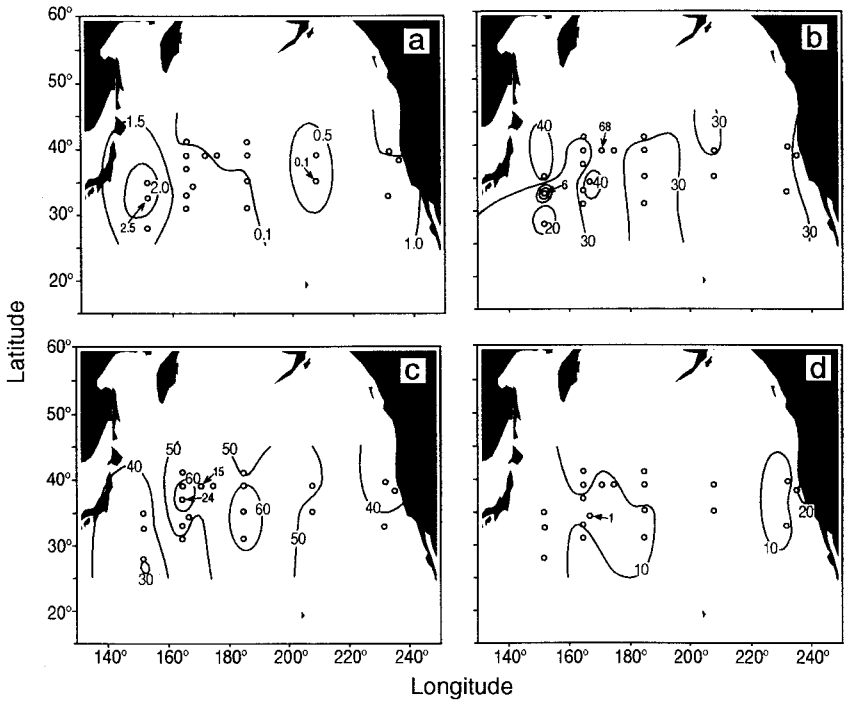

FIG. 5. (a) Log_{10} of the water column average kinetic energy per unit mass in the North Pacific Ocean. (b) Percentage of water column average kinetic energy per unit mass found in the barotropic mode. (c) Percentage of water column average kinetic energy per unit mass found in the first baroclinic mode. (d) Percentage of water column average kinetic energy per unit mass found in the second baroclinic mode.

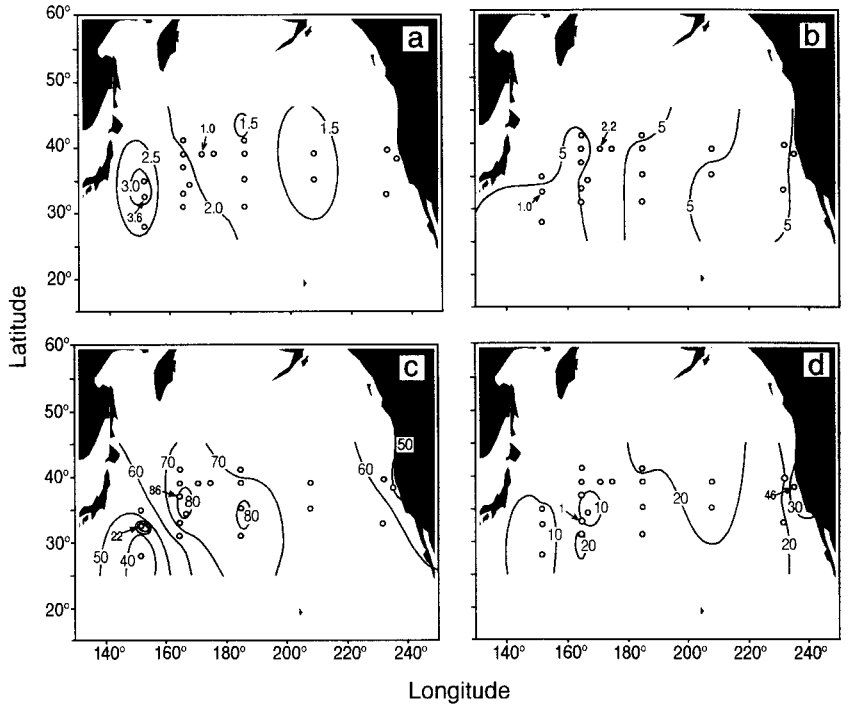

FIG. 6. (a) Log_{10} of estimated surface kinetic energy per unit mass. (c–d) Same as in Fig. 5c–d except for the surface kinetic energy per unit mass $T^{(2)}(0)$. Owing to the surface intensification of the baroclinic modes, little of the surface kinetic energy is barotropic.

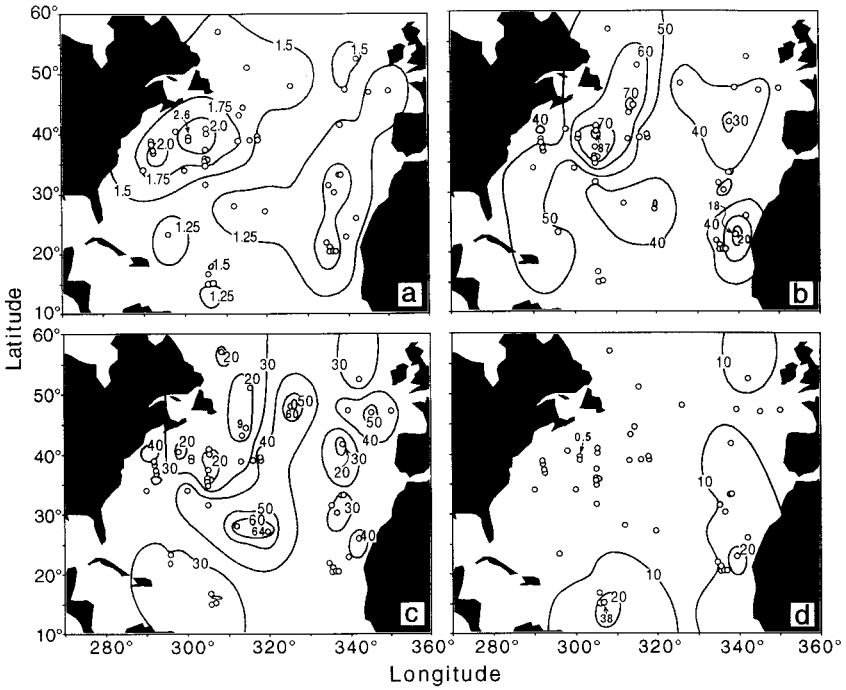

FIG. 7. (a–d) Same as in Fig. 5a–d except for the North Atlantic.

barotropic, but reaching an extreme near 90% just south of the Gulf Stream. (That such extremes are not seen in the Pacific may be a function of the failure to obtain data in the equivalent dynamical area of the Kuroshio, the southern recirculation regime.) A ridge of strongly barotropic motion extends along the entire east coast of North America. The first baroclinic mode is correspondingly reduced in the Gulf Stream area and on the western side of the ocean generally, but displays a midoceanic maximum of around 55% reaching to 65%, a feature

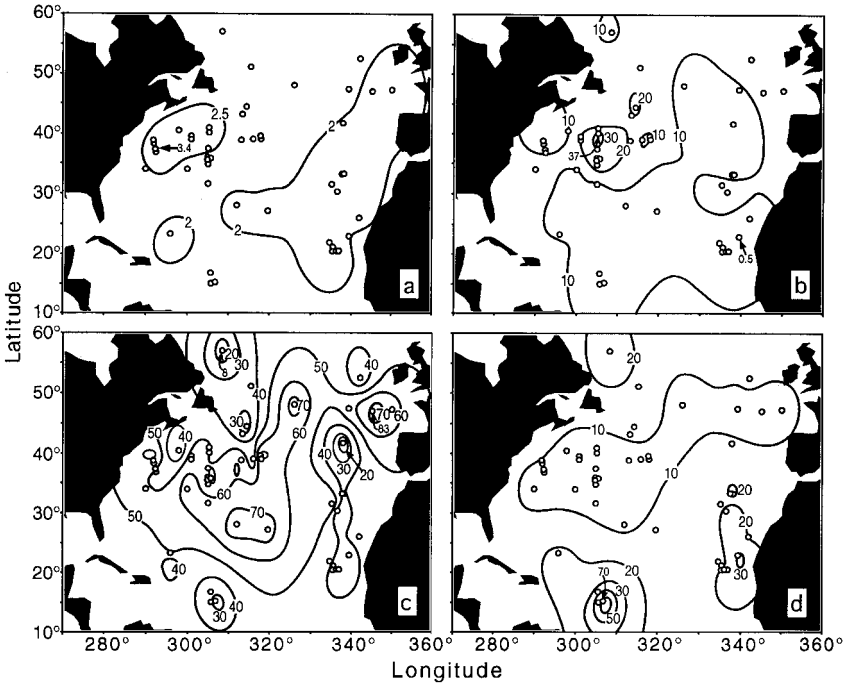

FIG. 8. (a–d) Same as in Fig. 6a–d except for the North Atlantic.

evidently lying over the Mid-Atlantic Ridge [see the discussion in Fu et al. (1985) of the effects of the ridge on the vertical structure of currents]. The second mode appears to play a stronger role in the Atlantic on the eastern side and toward the equator. Currents in the eastern North Atlantic subtropics are, however, very weak and variable (see discussion below).

As noted, the South Atlantic is only marginally contourable (Figs. 9 and 10) and the interior values are nothing but the mean of the available records. The Brazil Basin moorings show lower kinetic energy than in the Agulhas area and relative to the single mooring analyzed near 47°S in the Falkland/Malvinas trench. The Agulhas region is strongly barotropic, the Brazil Basin weakly so. In general, the Brazil Basin modal fits are poor and they strongly violate our a priori hypothesis. (As described in appendix B, the modal percentage confidence limits in this region all approach 100% owing to the vertical instrument distribution.) Note that these moorings were, on average, placed in atypical topographic settings. The first baroclinic mode in the Agulhas region contains most of the energy not contained in the barotropic mode with surprisingly little first-mode energy in the Brazil Basin. The second and higher baroclinic modes are important in the Brazil Basin but not elsewhere.

There are two isolated equatorial moorings, one in the Pacific and one in the Indian Ocean, which do not appear on the contour maps. In the Pacific, the barotropic mode is nearly absent from the total kinetic energy (about 5% in both components of flow) with the first baroclinic mode having about 50% of the energy, the remainder appearing in high modes. This behavior is consistent with the known high wavenumber structure of low-frequency motions on the equator (e.g., Eriksen 1985). Note that the low-latitude Atlantic moorings show a growth in the higher mode energies, although we did not have available a suitable equatorial mooring there. In the Indian Ocean, the mooring shows a nearly uniform modal distribution across the five-mode fits, in both components, again in contrast with the midlatitude results and consistent with known equatorial behavior. (A number of equatorial Indian Ocean moorings were obtained after the analysis reported in this paper was completed. These are listed at the end of Table 1, along with a few additional such moorings.)

The reliability of the modal decomposition varies enormously from mooring to mooring, depending upon duration and, especially, instrument vertical placement. To obtain an estimate of the reliability of the results, an approximate confidence limit was computed for each mode on each mooring as described in appendix B. The volume of numbers so generated is very large: there are 5 upper and lower limits for each mooring. These values are not displayed here, but some of the general properties of mooring types are briefly described in appendix B (the values are available from the author).

7) Surface kinetic energy

Figures 6a, 8a, and 10a show the logarithm of the surface kinetic energy $T^{(2)}$ (0) and the modal fractions. The surface kinetic energies can be compared directly to the values obtained from the altimeter. Figure 11 (taken from Stammer 1997) shows the global distribution of altimetric kinetic energy, and Figs. 12 and 13 show a regional expansion of the global result to correspond with the similarly colored current meter results. The reader is reminded that the altimeter result is from a uniform three-year coverage, spatially averaged over 2° everywhere, while the current meter results are of inhomogeneous duration, are based upon an extrapolation to the sea surface, and assume temporally uncorrelated vertical modes. Thus, the general agreement between the current meters and the altimeter is quite pleasing (with one exception) and at least qualitatively supports both the vertical extrapolation of the current meter values and the interpretation we are about to put upon the altimeter results.

The most conspicuous lack of agreement between the altimeter and the current meters lies in the western Pacific near 35°N where the current meters fail to display the long tongue of high kinetic energy so apparent in the TOPEX/POSEIDON data. Although several possibilities exist for rationalizing this difference including some unusual near-surface dynamics there, the most plausible explanation lies with the assumption of isotropy, which was made by Stammer (1997) to compute the altimetric kinetic energy. The actual extent of isotropy in this region is unclear from the current meter moorings. For example, the southernmost of the two moorings lying within the tongue (designated number 28) actually shows more energy in the meridional component of variability than in the zonal. But the kinetic energy of the record mean is 36 times larger in the zonal component than it is in the meridional component of the shallowest instrument (168 m). Because the record is only one year long, one cannot evaluate the actual degree of isotropy there. Furthermore, longer records would surely display much more variability energy than is seen with only one year. (Altimetric cross-over points, where two nonorthogonal velocity components are available, might be the best way to obtain useful values.) It is also possible that there is a failure of the temporal noncorrelation hypothesis and that the modes are phase coupled so as to intensify the surface motions. Although the phase-locked estimated surface kinetic energy $T^{(1)}(0)$ is larger than $T^{(2)}(0)$ (not shown), it does not bring the values up to those depicted by the altimeter. But it seems premature to conclude that there is any real paradox at this time—reducing altimetric kinetic energy by a factor of 2 would remove the most intensely red contour of the Kuroshio Extension in the lower part of Fig. 12, eliminating the problem. Conversely, raising the current meter value by a factor of 2 would produce a similar feature.

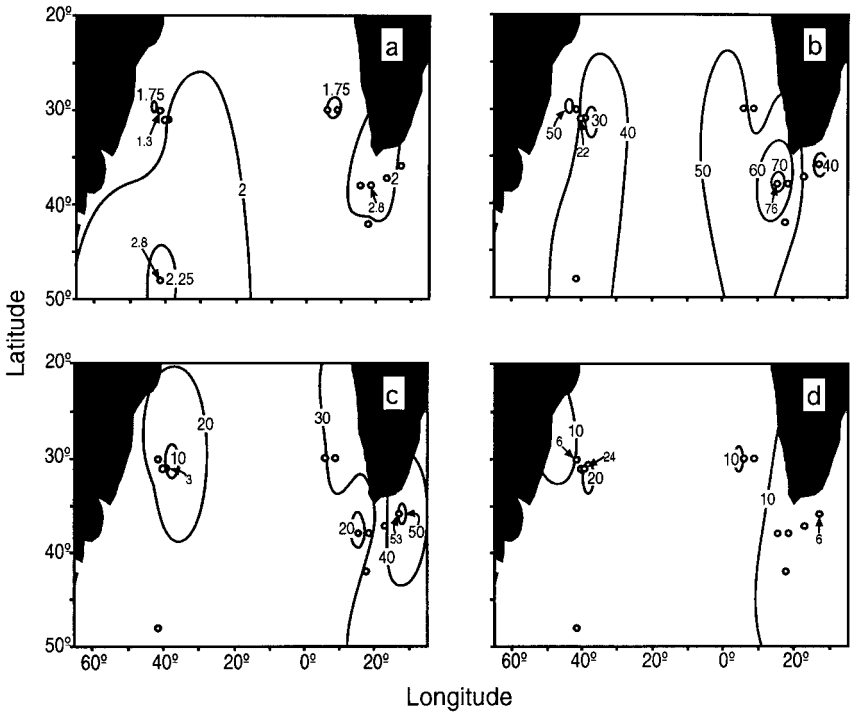

FIG. 9. (a–d) Same as in Fig. 5a–d except for the South Atlantic. Interior ocean values are just the mean of the mooring values.

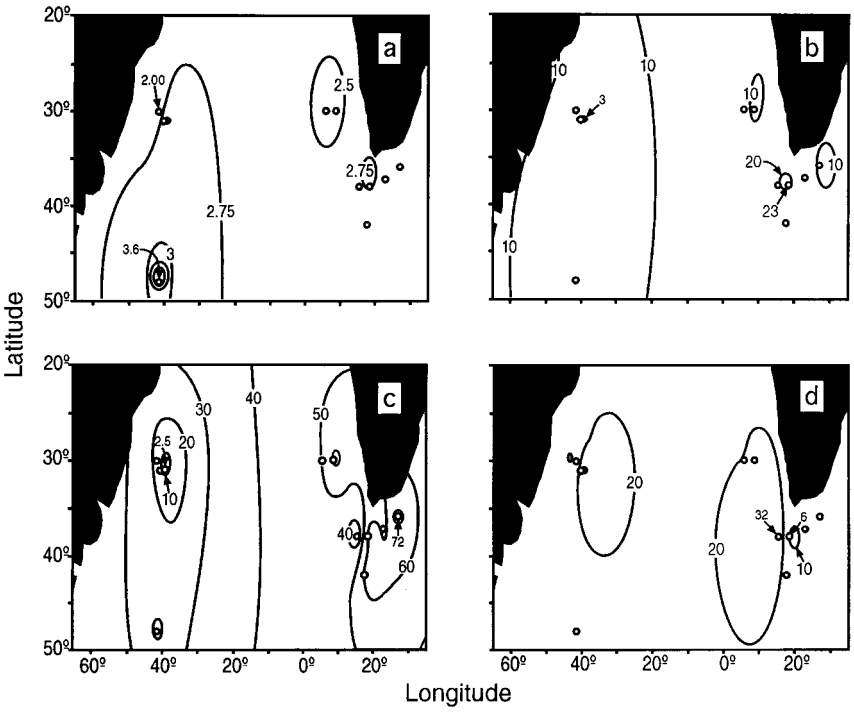

FIG. 10. (a–d) Same as Fig. in 6a–d except for the South Atlantic.

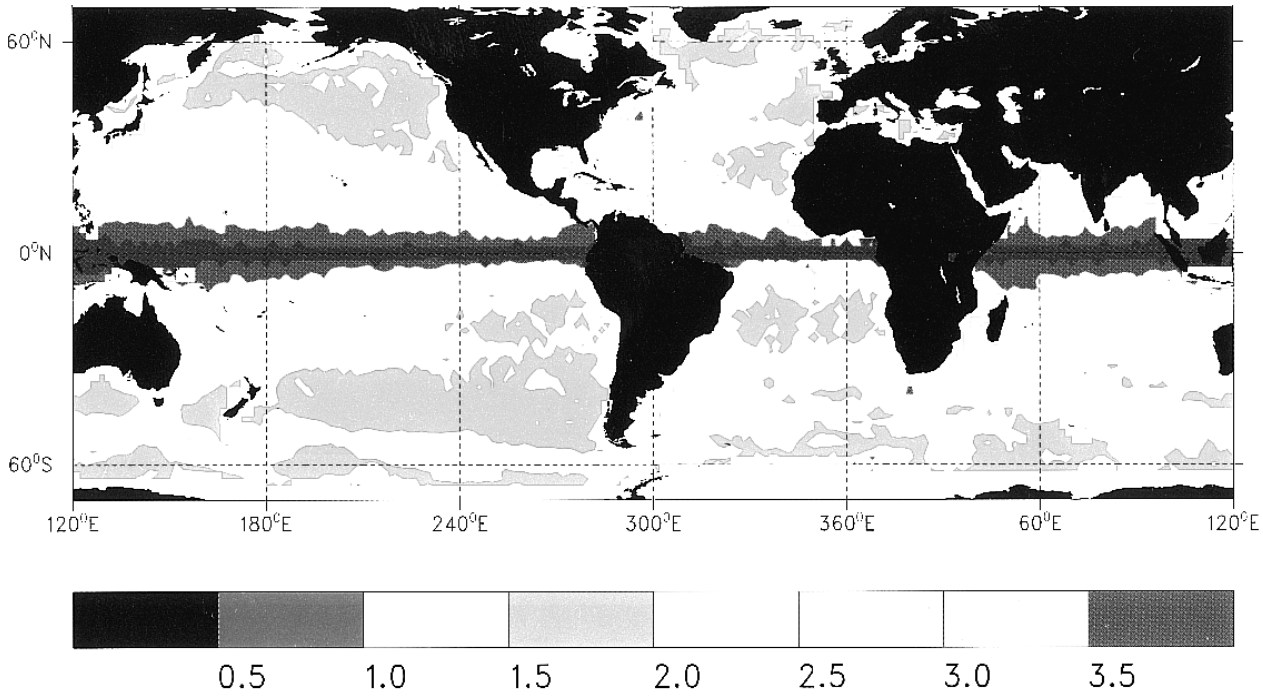

FIG. 11. Global surface geostrophic kinetic energy as estimated from the local slopes of three years of TOPEX/POSEIDON data (Stammer 1997) using the assumption of horizontal isotropy.

The maximum and minimum surface kinetic energies per unit mass coincide spatially with the maximum and minimum of the water column average kinetic energy. In the North Atlantic the maximum occurs in the Gulf Stream system with a value of about 2500 $cm^2\ s^{-2}$ and in the North Pacific the maximum is near 4000 $cm^2\ s^{-2}$. The North Atlantic value is roughly consistent with estimates from drifters [Richardson (1983); whose highest contour is 2000 $cm^2\ s^{-2}$ in this area], which would imply that the ageostrophic contribution to surface flows is comparatively weak there. Richardson's (1983) minimum contour is 200 $cm^2\ s^{-2}$, somewhat higher than the TOPEX/POSEIDON values. Brügge (1995) suggests that Richardson's values are generally too high in weakly energetic areas owing to his use of drifters that had lost their drogues. Brügge's values are closer to the altimetric values in the eastern North Atlantic and, in principal, the difference could be used to estimate the energy of the near-surface ageostrophic flows. Several efforts are under way to produce more detailed comparisons of surface drifter and altimetric kinetic energies and it seems premature to speculate about the results at this time.

Only one mooring, that at 34°N, 70°W, from the LOTUS experiment (Lippert and Briscoe 1990), carried current meters close enough to the surface to study the very near-surface behavior of the horizontal flow. The fitting results are shown in Fig. 15, which displays the u and v components of kinetic energy both $T^{(1)}(0)$ and $T^{(2)}(0)$ as a function of depth. The modal fit actually fails near the surface, at least in terms of the a priori value of σ_n^2,and the results were downweighted, although visually the fit is actually quite a good one (σ_n^2 may well be larger near the surface). To the extent the flow remains geostrophic near-surface, the modal phase locking tends to reduce the near-surface kinetic energy, as observed. Data are lacking, however, to pursue this subject of near-surface behavior any further here

The modal decomposition of the surface kinetic energy shows (Fig. 6), as expected, that the barotropic component is much reduced relative to the baroclinic ones. In the central North Pacific the surface values are dominated by the first baroclinic mode, with the contribution approaching 90% near 162°E and generally being over 60% over most of the mappable region. The second baroclinic mode appears important only near the U.S. West Coast (approaching 50% at a mooring shallower than the water depth selection criterion). The North Atlantic (Fig. 8) shows a barotropic component of about 10%, except that the water column means in the near Gulf Stream area are so strongly barotropic that a significant (near 40%) contribution remains in this mode there. The Mid-Atlantic Ridge remains as a region of strong first baroclinic mode contribution, near 70% over much of that area, with the first mode declining in the weaker kinetic energy areas of the eastern basin. The second baroclinic mode is important at the eastern boundary near Africa, and apparently in the North Equatorial Current area near 15°N.

In the Pacific, the single equatorial mooring shows

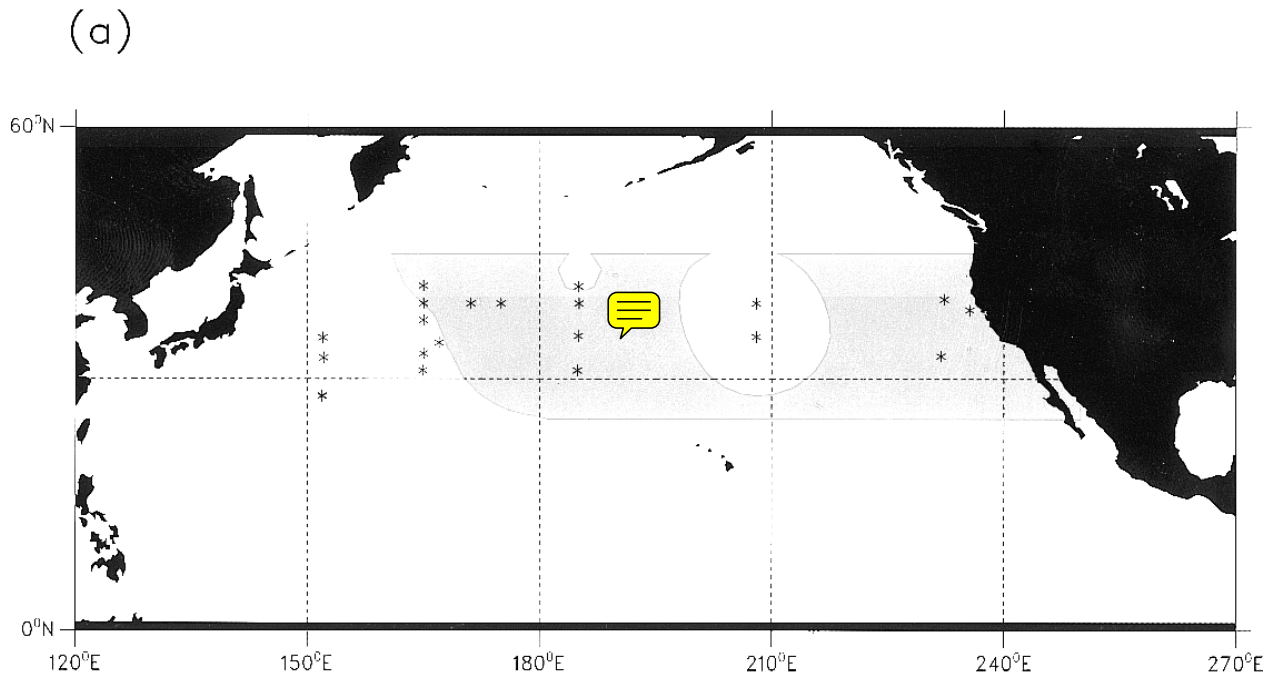

FIG. 12a. Results in Fig. 11 expanded in the region of North Pacific current meter data coverage.

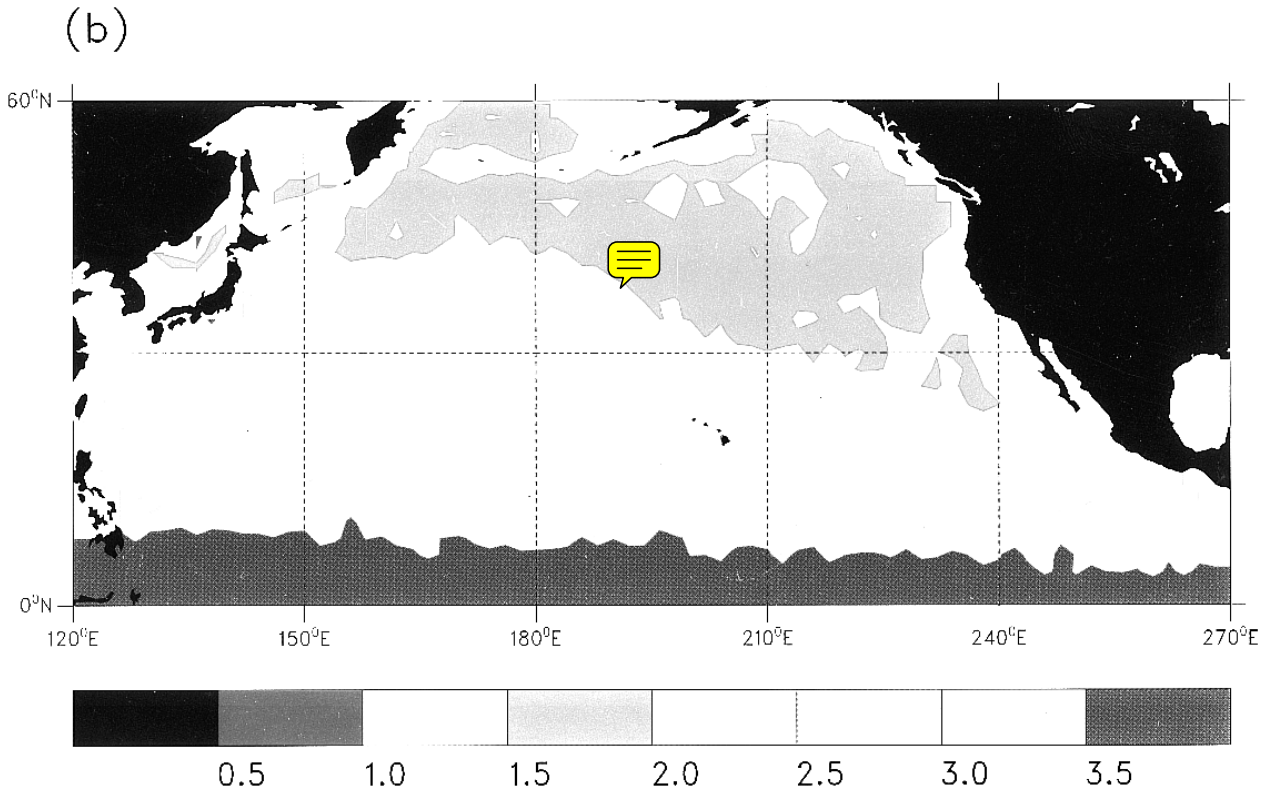

FIG. 12b. As in Fig. 12a but as estimated ($T^{(2)}(0)$) from the current meters rather than the altimeter.

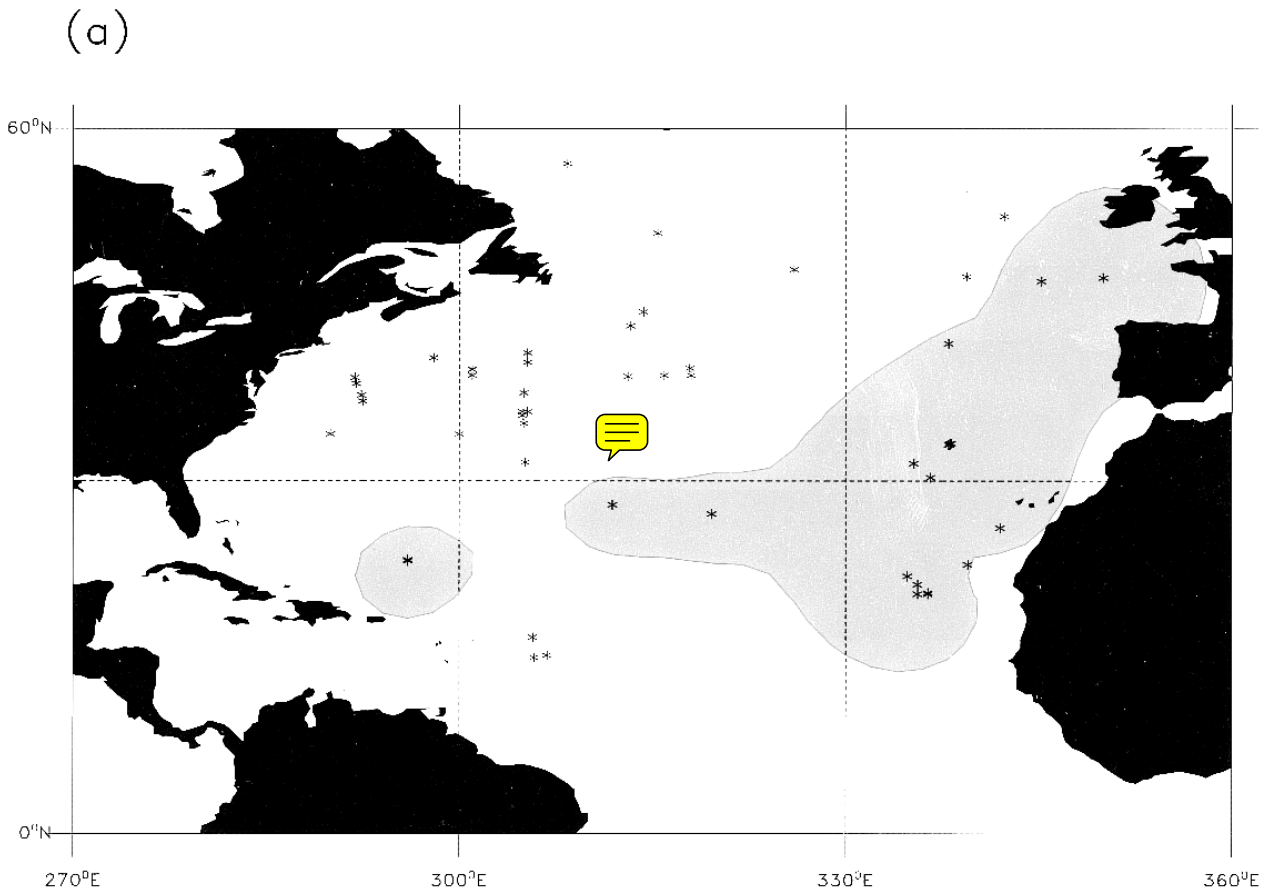

FIG. 13a. As in Fig. 12a except for the North Atlantic.

about 50% of the surface kinetic energy is in the first baroclinic mode, but in the Indian Ocean only about 25% is in that mode. The estimated barotropic contributions are negligible. For altimetric interpretation, these regions require special discussion relative to the higher latitude results.

These results for the surface kinetic energy provide an immediate rationalization of the negative outcome of the search by Gaspar and Wunsch (1989), Fu and Davidson (1995), and Chechelnitsky (1996) for skill in barotropic model estimates of sea surface variability: the altimeter sees very little barotropic kinetic energy. [The situation may well be different for elevation (potential energy), rather than the slope (kinetic energy).]

8) ANISOTROPY AND TIMESCALES

We are far from having exhausted the structure of our results. As already noted, each current meter record, and hence each mode, is described by a frequency spectrum. Many of these spectra exhibit complex structures, and the energy levels alone cannot fully describe such records. [It is worth recording the nearly universal behavior that at high frequencies (periods generally shorter than about 10 days) modal equipartition is seen, and all indications are that at these short periods, there is a nearly ''white'' modal structure with a behavior consistent with a fully turbulent field.] We have also suppressed discussion of the differences between the zonal and meridional components of flow—even though some record exhibit considerable anisotropies in the relative energy levels.

Because the database here consists of current meter records, the focus has been on the horizontal kinetic energy spectrum, which is related to the altimetric slope spectrum. On the basis of the altimetric results (Wunsch and Stammer 1995, Stammer 1997), one expects the mesoscales to dominate the result (see, e.g., Fig. 6 of Wunsch and Stammer 1995), but the actual spectral distribution is expected to vary strongly with region. In lieu of a complete display of frequency power density spectra for each mode of each component of velocity, Fig. 15 depicts the timescale for the meridional and zonal components of velocity in the separate barotropic and baroclinic modes in the Atlantic. The timescale was defined as in Eq. (8),

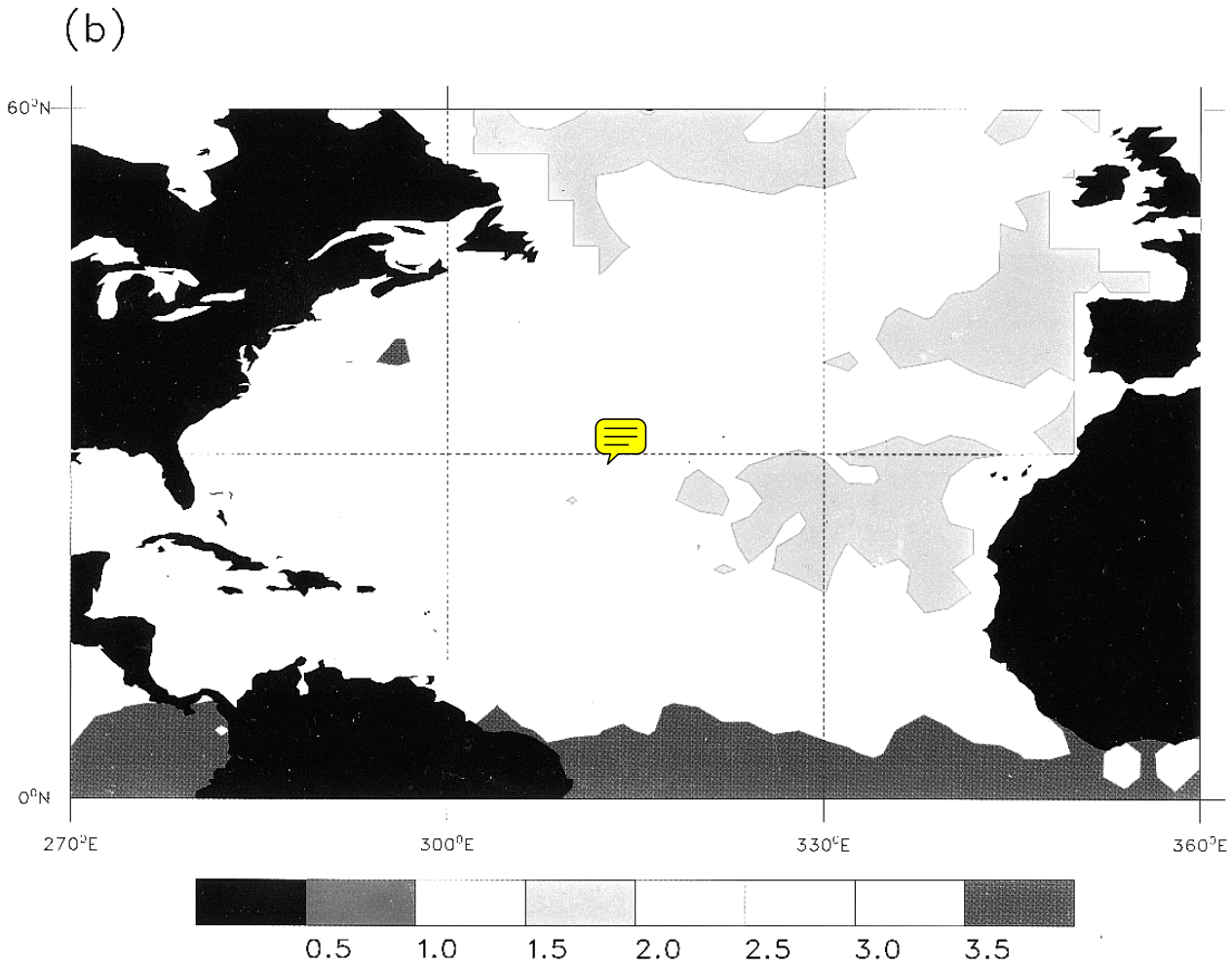

FIG. 13b. As in Fig. 13a except from the current meters. If the Labrador Sea current meters are not downweighted, the orange band of high energy extends into that region, wrapping around the Tail of the Banks.

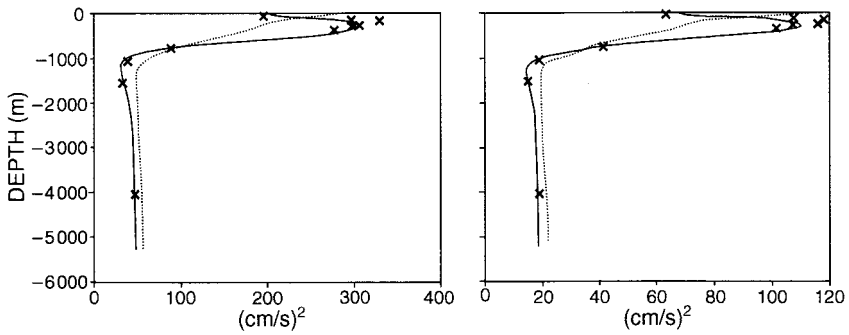

FIG. 14. The vertical profiles of kinetic energy in the zonal (left panel), and meridional components (right panel) for the LOTUS mooring at 34°N, 70°W. This mooring had, exceptionally, 10 useful records, primarily distributed in the upper ocean. Solid line depicts the kinetic energy $T^{(1)}(z)$ in which no modal decoupling hypothesis is made. Dashed line shows $T^{(2)}(z)$ in which the modes are assumed temporally uncorrelated; "×" is the measured kinetic energy at each instrument. With a perfect fit, the solid line should pass through each such point. Here the modal coupling is such as to reduce the surface kinetic energy density relative to that below. The modal fit is a relatively poor one just below the surface.

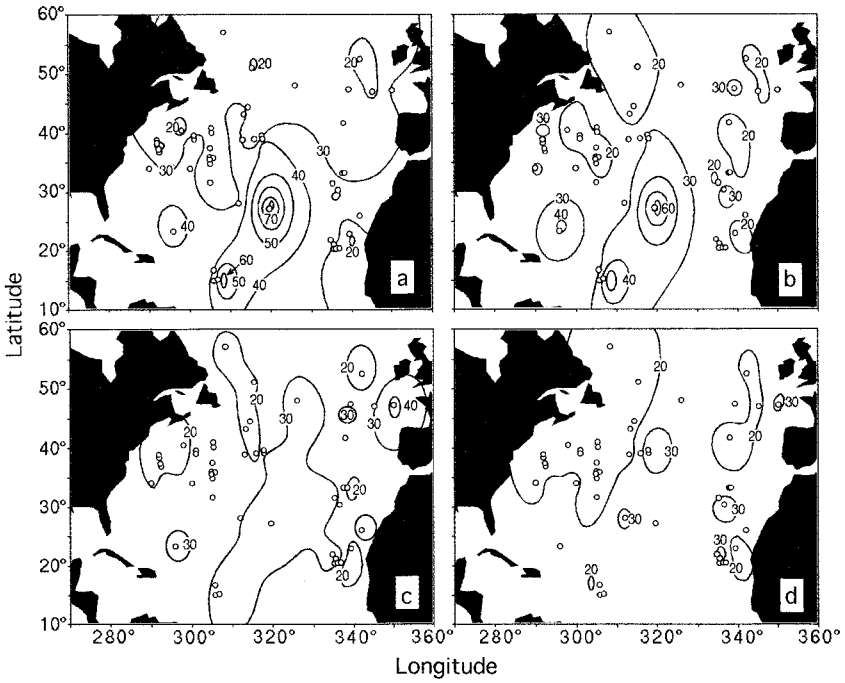

FIG. 15. Decorrelation timescales, as defined in the text, for (a) the barotropic mode, zonal component; (b) barotropic mode, meridional component; (c) first baroclinic mode, zonal component; and (d) first baroclinic mode, meridional component.

$$T = \Delta t\left(\tilde{R}(0)^2 + 2\sum_{j'\geq 1}\tilde{R}(j')^2\right)\Big/\tilde{R}(0)^2, \qquad (13)$$

where the computation was carried out for each component and mode separately and Δt is the time step (one day). Here the summation on j' was taken over terms satisfying the requirement that $\tilde{R}(j') > \tilde{R}(0)/N$ (Priestley 1981)—a rough level of no significance for a sample covariance. Equation (13) is an approximation to a *decorrelation* timescale and is not necessarily the dominant timescale of the motions.

In the zonal component, Fig. 15 shows the Mid-Atlantic Ridge region to be one of extended timescales, around 50 days in both barotropic and first baroclinic modes. Otherwise, the timescale is around 20 days, with growth toward the Tropics. In the meridional component, there is a mild indication of the Mid-Atlantic Ridge in the barotropic component alone, while the first baroclinic mode shows little structure apart from a shortening of timescale in the Labrador Sea/Gulf Stream area. In the Pacific (not shown), the timescales are generally longer; for example, being around 50 days for the first baroclinic mode in the *u* component. These timescales are all consistent with the prior supposition of dominance by mesoscale variability.

Stammer (1997) displays timescales computed from the TOPEX/POSEIDON data. These differ from the present computation in a number of ways: necessarily, Stammer's computation is an average from all the modes; the values are for elevation rather than velocity; and the timescale was defined from the integral of the autocorrelation to its first zero-crossing rather than from Eq. (13), which accounts for true correlation beyond that point. The timescales we find here are generally considerably longer than those determined by Stammer (1997). Despite all these differences, however, the rough *patterns* of the timescale are reproduced: in the Atlantic, timescales are longer over the Mid-Atlantic Ridge with a sharp decrease in the subpolar gyre and in the Gulf Stream region, and a decrease from the subtropical gyre toward the Spanish coast. In the Pacific, the region north of Hawaii has longer timescales than elsewhere, with general declines toward both coasts.

The current meters are generally not useful for defining horizontal spatial scales. Most simultaneous mooring deployments produced records that are incoherent. The spatial structure is inferable only from the altimeter data and from models.

b. Problematic results

Although the great majority of moorings are at least crudely consistent with the prior hypothesis and suggest that the modal fits are adequate, there are several interesting failures, some of which have already been alluded to. There are several classes of difficulty:

1) *Overshoot in the fit.* Figure 16 shows a problematic fit, given a low subjective weight, where a distinct ''overshoot'' takes place between observation po-

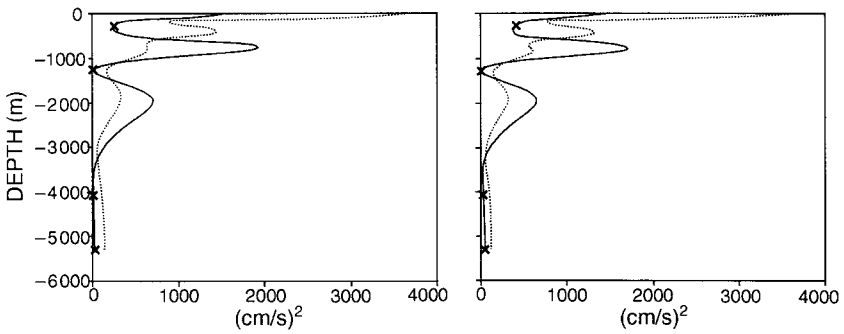

FIG. 16. Example of a fit that ''overshoots'' in both zonal (left panel) and meridional components (right panel). The mode coupled kinetic energy $T^{(1)}(z)$ (solid line) is small at the observation positions but becomes quite large where unconstrained. Dashed line is $T^{(2)}(z)$. This is an extreme example, and the result was severely downweighted.

sitions. This behavior is common in moorings with a poor instrument distribution.

2) *Intermittent temporal misfit.* Figure 4 shows a modal fit that is generally quite good, failing intermittently during the data duration owing, typically, to energetic events of comparatively brief duration. Such records were not generally downweighted because on average the fit is a good one.

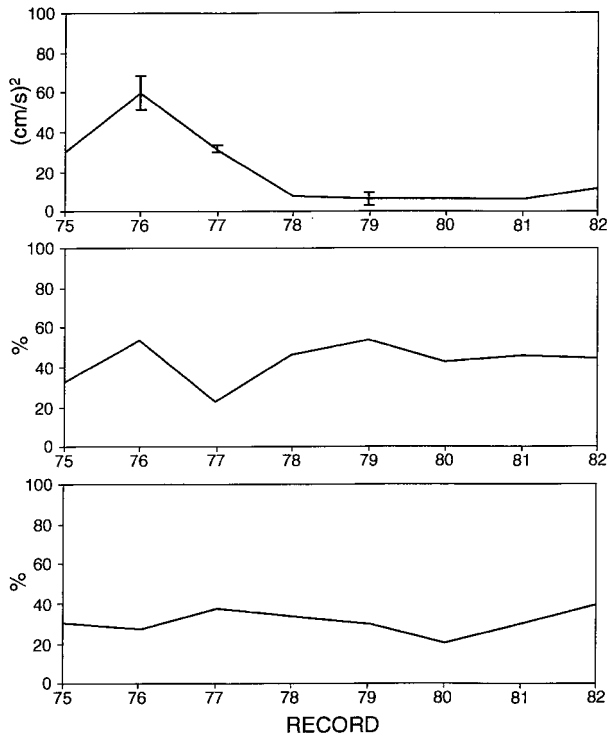

FIG. 17. Time variability of the logarithm (base 10) of the kinetic energy per unit depth (upper panel), and of the percentage found in the barotropic mode (middle panel) and the first baroclinic one at the site of the long-running Kiel mooring in the eastern Atlantic basin. Each data point represents about 295 days of record. Such time variations appear most marked in weakly energetic regions of the ocean, but generally support the idea that many years of data are required to obtain statistically stable results at any specific location.

3) *Temporal instability.* Scientists at the University of Kiel (Müller and Siedler 1992) maintained a mooring near 33°N, 22°W for many years, permitting examination of the stability of the results over time. Figure 17 shows the change in kinetic energy and the energy fraction in the barotropic and first baroclinic modes (average record duration is about 295 days). Müller and Siedler (1992) noted the general instability of the statistics here. Considerable changes are observed, hence requiring the spatial averaging we have done in depicting our results. A caveat, however, is that, as in the Brazil Basin, results from these weakly energetic deep basins are generally much less stable than elsewhere, spatially as well as temporally. As already noted, Schmitz (1989) pointed out temporal changes over a decade in energy levels in the so-called MODE area, and the TOPEX/POSEIDON altimeter is beginning to show considerable interannual fluctuations in kinetic energy levels (e.g., White and Heywood 1995).

4) *Failure of the modal ratio hypothesis.* Although we have done no formal statistical tests, the a priori modal partitioning is clearly seen to fail qualitatively in a number of locations. Most conspicuous is the Brazil Basin region where, for the three moorings analyzed, the energy contained in the barotropic and first baroclinic modes is comparatively weak, the third and fourth modes contain comparatively large amounts of energy, and the fits are generally poor (see Table 1). Other, isolated, locations with strong high-mode contributions can be inferred from the table as the places where the first two modes contain a small fraction of the energy. In many cases, including the Brazil Basin moorings, where some are actually in the Vema Channel there are topographic peculiarities, which are expected to produce complex results.

5) *Strong temporal modal correlations.* The finding of strong correlations is not, per se, a difficulty, but a result. A measure of the degree of modal coupling lies in the ratio of the two definitions (10), (11) of

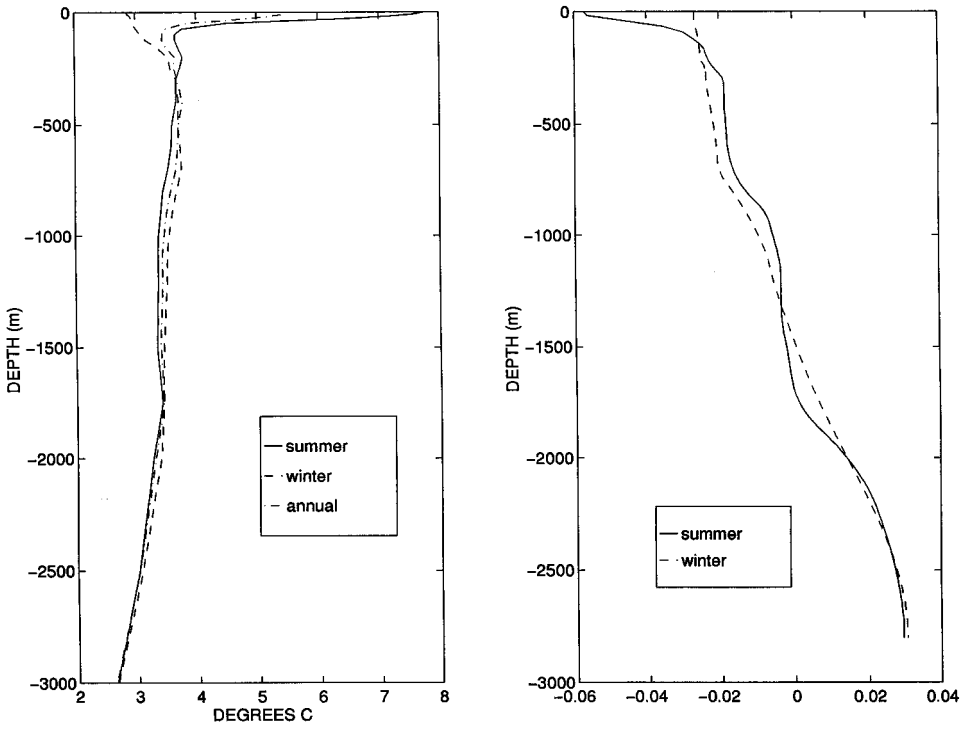

FIG. 18. (Left) Summer, winter, and annual mean temperature profiles in the Laborador Sea near mooring 57°N, 51.6°W and the seasonal change in the near-surface behavior of the first baroclinic mode (right), which is much more intensely amplified in the summer.

surface kinetic energy. They are within a factor of about 3 of each other over most of the ocean, but very large excursions in both directions do occur as can be seen in Table 1. Maps (not shown) were prepared of the ratio in the North Pacific and North Atlantic. In the North Pacific the entire region is one where mode locking increases $T^{(2)}(0)$ relative to $T^{(1)}(0)$, on average by about 50% or less. A conspicuous exception is the mooring described by Hamann and Taft (1987) at 39°N, 171°E in the Emperor Seamount Experiment. This mooring was strongly downweighted because the correlated and uncorrelated kinetic energy profiles were radically different, and inclusion of the fully weighted results in the various maps grossly distorted them in the immediate vicinity of this mooring, which is clearly anomalous. [$T^{(2)}(0)$ greatly exceeds $T^{(1)}(0)$.] Another Pacific extreme occurs at the mooring near 37°N, 171°E. This mooring, which exhibits other peculiarities (a large eddy heat flux), has $T^{(2)}(0)$ exceeding $T^{(1)}(0)$ by a factor of 30.

In the North Atlantic, the patterns of phase locking change across the Mid-Atlantic Ridge. East of the ridge $T^{(1)}(0)$ generally exceeds $T^{(2)}(0)$—quite significantly just west of Africa—while west of the ridge the ratio is reversed, but with some small-scale fluctuations crossing the Gulf Stream. Otherwise, the extremes of apparent modal coupling occur at the two moorings in the northwest Atlantic at 51.1°N, 44.6°W, and 57°N, 51.6°W, where the modal coupling serves to strongly decrease the surface value and, somewhat surprisingly, in the Nares abyssal plain moorings (numbers 2, 52, 53), where $T^{(2)}(0)$ greatly exceeds $T^{(1)}(0)$.

6) *Strong seasonal fluctuations.* The mooring at 57°N, 51.6°W is anomalous in a number of other ways. In this region there is a very strong seasonality to the temperature profile (Fig. 18), which leads to a strong seasonality in the amplification of the baroclinic modes near the surface (Fig. 18b). Here a much longer record needs to be analyzed by season, and one can infer that the coupling to the wind field will be quite different in winter than in summer. The results in the table and maps are from the annual mean conditions, which tend to more resemble the summer period than the winter one.
7) *Large vertical mooring displacements.* Many of the moorings deployed in the vicinity of strong currents are often deflected vertically by very large amounts (e.g., Fig. 19), particularly when the flows are dominantly barotropic. Results from all such moorings are biased, either because the nominal assigned depths do not correspond to the actual depths during the most energetic events and/or because data are missing entirely during such events. We have no immediate remedy for such difficulties, and the reader is warned that results from current meter moorings in highly energetic regions may be badly distorted

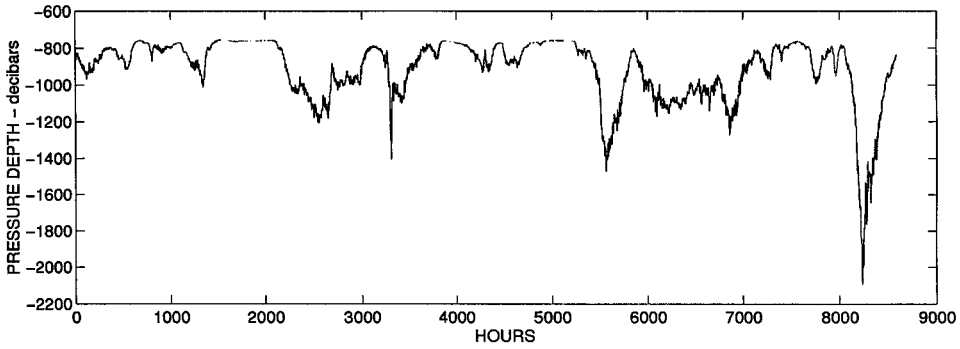

FIG. 19. Pressure record from a mooring near 39°N, 59°W showing large excursions. Such records are typical from moorings in and near the Gulf Stream and lead to potentially significant bias in all results reported from such records

(this warning applies to all results reported from such moorings, not just the present ones).

4. Empirical orthogonal functions

From the earliest studies of moored current meter mooring data (e.g., Inoue 1985; Mercier and Colin de Verdiere 1985; Müller and Siedler 1992; and many others), various forms of so-called empirical orthogonal functions have been used to produce efficient depictions of the vertical structure of the motions. This representation of all of the moorings analyzed has also been computed here, but owing to the conclusion drawn that they can be very misleading, the results are relegated to appendix A. The fundamental issue, as described in appendix A, is that for many moorings the lowest EOF appears to be a combination of the barotropic and first baroclinic modes, and the conventional interpretation has been that this form indicates a strong coupling (correlation in time) between these two dynamical modes. But as shown in appendix A, this interpretation can be quite erroneous. Furthermore, the EOFs cannot be extrapolated in any straightforward way to the sea surface.

5. Summary and concluding remarks

As stated in the introduction, the ultimate intent is to extend the horizontal wavenumber–frequency spectra of Wunsch and Stammer (1995) to include the vertical dimension as well. This work will be published elsewhere. But the global picture that emerges from the current meters alone—imperfect as it is and with many caveats—is fairly simple and useful:

1) The inference of the surface geostrophic flow fields from altimetry and from vertical extrapolation of current meter records expanded in modes are generally consistent. The single visual exception is in the Kuroshio Extension where the altimeter portrays surface intensification not apparently seen by the current meter moorings. The most likely explanation is the failure of the isotropy assumption used to compute altimetric kinetic energy and/or the too-short record lengths.
2) As inferred from earlier regional studies, the barotropic and first baroclinic modes dominate the water-column-average kinetic energies except in the Tropics.
3) Surface kinetic energies are dominated by the first baroclinic mode, and thus to a first approximation, the altimeter over much of the World Ocean is directly reflecting the movement of the main thermocline. Although it has not been discussed here, one can relate the vertical displacements of the isopycnals in each mode, $G_n/(-i\sigma)$ at frequency σ, owing to either component of horizontal velocity, to the corresponding horizontal mode $F_n(z)$ through relations of the form

$$G_n(z)/(-i\sigma) = \frac{1}{N^2(z)}\frac{dF_n(z)}{dz}, \tag{14}$$

where $N(z)$ is again the buoyancy frequency. Note, however, that the quantitative vertical displacements depend upon the numerical values of the horizontal structure of the motions; see, for example, Wunsch and Stammer (1997). From (14), the estimated mean-square kinetic energies at each mooring, and the horizontal wavenumber spectrum one can readily infer the mean-square displacements at each mooring. [The conclusions drawn here contradict those of a recent paper by Woodgate and Killworth (1996) who infer that altimetric data could not be used to determine the subsurface density field perturbations, while we encounter no particular difficulties in making inferences about the interior motions. Our a priori assumption that the barotropic mode has finite energy prevents it from producing the spurious interior density perturbations that troubled them.]
4) Barotropic models of sea surface variability should show little or no skill—consistent with the previously published results. This conclusion does not necessarily apply to regions where no current meter records have been available.

In section 2a it was noted that the results might differ significantly if we used not the vertical modes of a resting ocean, but rather one with a near-surface intensified zonal mean flow $U(z)$. Such modes, neutral or otherwise, are an intimate part of studies of oceanic baroclinic instability (e.g., Gill et al. 1974). For a given $U(z)$, $N(z)$ one can find the neutral modes and use them for expansion of the observed velocities. Several reasons, however, militate against their use here: (i) few, if any, observed current meter averages are statistically significant—precluding a reasonable estimate of $U(z)$; (ii) such modes, unlike those for $U = 0$, are dependent upon the lateral scales of motion, which are unknown from single current meter moorings; and (iii) the semiquantitative agreement of the altimetric and mode-extrapolated surface kinetic energies suggests that the use of $U(z) \neq 0$ is unnecessary to describe the existing dataset.

The present analysis nonetheless can be extended and improved in a number of ways, including use of moorings not analyzed here, and through more specific analysis at each mooring (e.g., using local values for the a priori noise in each instrument). It seems unlikely, however, that many more open ocean, long duration moorings with extensive current meter coverage will be deployed any time soon. In the long-term therefore, we anticipate that descriptive analyses such as the present one will be obtained from ocean general circulation models constrained to the time-evolving altimeter data (and other global-scale observations). The models, if consistent with the observations and representing known physics, then should have vertical energy distributions that can be analyzed in the same manner as the current meter moorings have been, and the result should provide better estimates of the partitioning in the real ocean. Existing models and estimation schemes are not yet adequate to claim either complete observational consistency or adequate physical representation (e.g., Stammer et al. 1996). Until they are, the present results become another test of the accuracy of models: We can compare the energy levels and vertical partition as seen in a model with the results obtained here.

The patterns of energy and energy partition that emerge also, of course, invite theoretical explanation. For example, the intense barotropic nature of the flow just south of the Gulf Stream and the first-mode dominance over the Mid-Atlantic Ridge are features for which physical mechanisms have been previously suggested. It remains to render the discussion quantitative.

Acknowledgments. It is a pleasure to acknowledge the help of several individuals whose efforts made this compilation possible. The data employed here were obtained from the WOCE Current Meter Data Assembly Center, which operates under the direction of D. Pillsbury; from Woods Hole Oceanographic Institution (with much assistance from S. Tarbell and N. Hogg); from the University of Kiel (through the efforts of T. Müller and F. Schott); from the University of Brest (A. Colin de Verdiere); the BEST records (A. Gordon and D. Pillsbury); from the University of Rhode Island (R. Watts), Bedford Institute of Oceanography (A. Clarke), Albert-Wegener-Institut (E. Fahrbach), U.S. Navy Research Laboratory (Z. Hallock), and from older records already on file at MIT. I am indebted to C. King, for assembly of the entire set in MATLAB readable form and general help. A. Whittemore and J. B. Keller provided the essential ingredients of the confidence limit calculation in appendix B. Supported in part by Contract 958125 with the Jet Propulsion Laboratory. D. Stammer and T. Müller made many helpful comments on the manuscript. Contribution to the World Ocean Circulation Experiment.

APPENDIX A

Empirical Orthogonal Functions

Here we take up the description of time-dependent motions on moorings in empirical orthogonal functions. Most representations have been in terms of purely time-domain EOFs although Mercier and Colin de Verdiere (1985) use the frequency domain form of complex EOFs (cf. Wallace 1972). Both are easily understood (e.g., Jolliffe 1986; Wunsch 1996) from the singular value decomposition (SVD). Here we use only the real case. Define the $L \times M$ matrix

$$\mathbf{U} = \underbrace{L \updownarrow\{ \mathbf{u}_1(t)\ \mathbf{u}_2(t) \cdots \mathbf{u}_M(t)\ \}}_{M}, \tag{A1}$$

whose jth column is the vector of time series of velocity component u_j at depth z_j. Then the Eckart–Young–Mirsky theorem produces the most efficient representation in a 2-norm of $\mathbf{U}$ as

$$\mathbf{U} \simeq \boldsymbol{\alpha}_{u1}\lambda_1^{\mathrm{T}}\boldsymbol{\beta}^{\mathrm{T}} + \cdots + \boldsymbol{\alpha}_K\lambda_K\boldsymbol{\beta}^{\mathrm{T}},$$

from all sets of K-orthonormal vectors

$$\boldsymbol{\alpha}_i^{\mathrm{T}}\ \boldsymbol{\alpha}_j = \delta_{ij},\ \boldsymbol{\beta}_i^{\mathrm{T}}\boldsymbol{\beta}_j = \delta_{ij},$$

if $\boldsymbol{\alpha}_{\ i}$, $\boldsymbol{\beta}_{\ i}$ are the singular vectors of $\mathbf{U}$, and λ_i the corresponding singular values. The representation is ''efficient'' in the sense that the norm of the difference;

$$\|\mathbf{U} - (\boldsymbol{\alpha}_1\lambda_1\ \boldsymbol{\beta}_1^{\mathrm{T}} + \cdots + \boldsymbol{\alpha}_K\lambda_K\boldsymbol{\beta}^{\mathrm{T}})\|$$

cannot be made any smaller for any other orthonormal sets of K vectors. For the particular definition of $\mathbf{U}$ in (15), the $\boldsymbol{\alpha}_i$ are the temporal EOFs and the $\boldsymbol{\beta}_i$ are the vertical ones. Note that weights are readily applied to $\mathbf{U}$ prior to determination of the singular vectors should that be desirable.

Figure A1a shows the first three time-domain EOFs of a mooring on the Nares abyssal plain. Separate fits are done for U, V. With four instruments, four EOFs account for 100% of the energy in the records; here three EOFs make up about 99% of the u-component variance [see Jolliffe (1986), for a discussion of the relationship between the singular values and the vari-

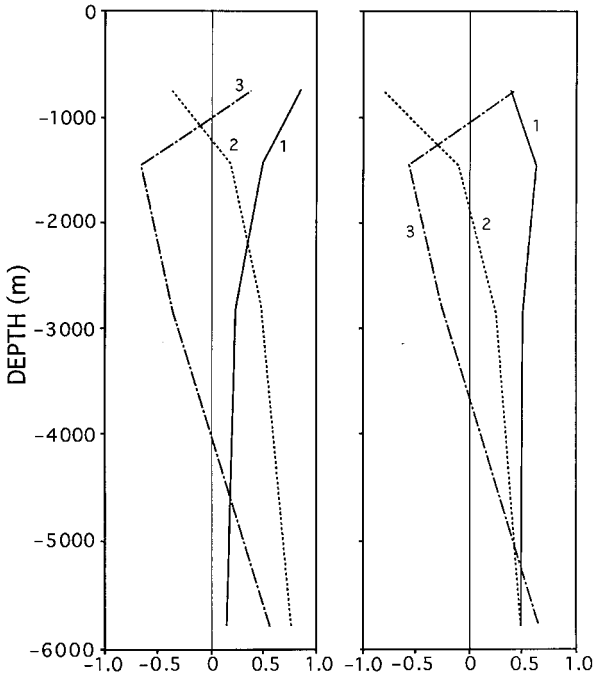

FIG. A1a. Typical EOFs (left panel for u, right panel for v) of the horizontal currents at a mooring near 23°N, 64°W. The first function for u looks like a sum of a coupled barotropic and first baroclinic mode, but as discussed in the text, this result can be an artifact of two such modes, which are uncorrelated but of nearly equal energies.

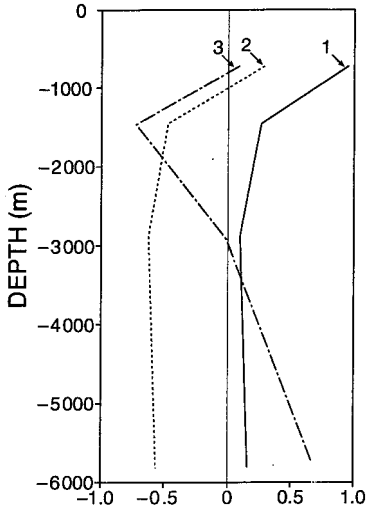

FIG. A1b. EOFs computed for artificial time at the positions of the instruments in the mooring of Fig. A2a, with the barotropic and first baroclinic modes present with equal energy, but generated as perfectly uncorrelated over the record duration. Note the emergence of an EOF appearing to be a phase-locked barotropic and baroclinic mode sum.

ance]. The first u-component EOF shown in Fig. A1a is typical of many that have been described previously in the literature, and which is common to many of the moorings employed here. The usual interpretation (going back, e.g., to Davis 1975) is that it is readily described as a linear combination of the barotropic and first baroclinic modes and, therefore, one is led to infer a coupling between these modes, and hence a significant nonlinearity in the system (McWilliams and Shen 1980). This interpretation may well be correct, but there are potentially fatal pitfalls.

To demonstrate the emergence of such an EOF under conditions of complete linearity, consider a synthetic example. Let $\xi_q(t)$, $1 \le q \le N$, be mutually uncorrelated zero-mean white-noise processes of uniform variance σ_ξ^2 and define the M time series as

$$u_i(t) = \sum_{q=1}^{N} F_{q-1}(z_i)\xi_q(t), \qquad 1 \le i \le M, \quad \text{(A2)}$$

that is, the synthetic record is the sum of N uncorrelated dynamical modes sampled at the depths of the current meters from the mooring used in Fig. 1. Records corresponding to (A2) were constructed from a pseudo-random number generator such that the variance of the barotropic and first baroclinic modes were equal, and that of the second to fourth baroclinic modes had half of their variance. The EOFs for this situation are shown in Fig. A1b with singular values λ_i = [0.88, 0.60, 0.43,

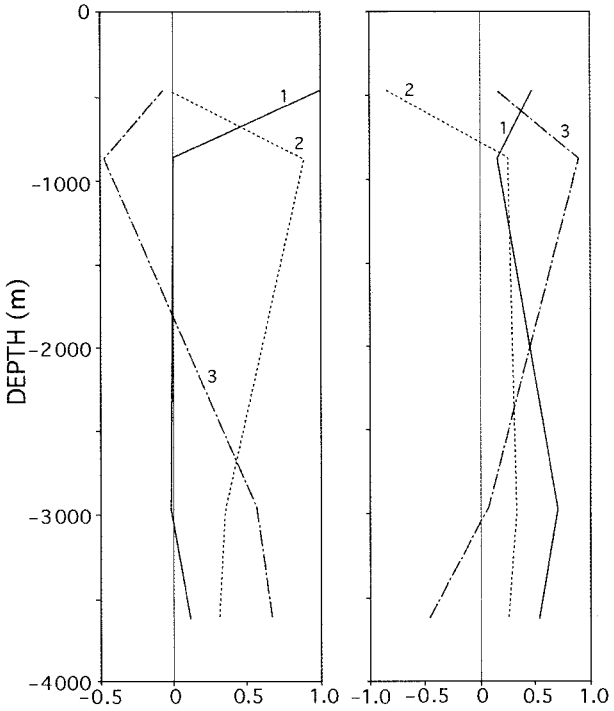

FIG. A2. First three EOFs of mooring number 71 in the Brazil Basin for u component (left) and of the v component (right) in which the lowest EOF differs markedly from either the barotropic or first baroclinic modes or their sum. This behavior is a symptom of a breakdown of the a priori mode hypothesis, but may only reflect the absence of middepth instruments.

0.08]. Note the emergence of a first EOF, which strongly resembles the sum of the barotropic and first baroclinic modes—in a situation in which they are present and are known to be uncorrelated. It is thus possible to be seriously misled concerning the actual dynamical situation.

There are several problems. Although the F_q are accurately orthogonal when integrated over the water column, they fail to be so when sampled at a small number of points. But the EOFs are by definition orthogonal in the vertical, and it is forced upon the system. Second, although the $\xi_q(t)$ are uncorrelated—a requirement equivalent to orthonormality in time—any finite realization produces a finite sample correlation. Again, the EOFs require rigorous orthogonality over the sample and will thus ''mix'' the modes so as to achieve it. Third, orthogonal bases are not unique in the SVD if two orthogonal modes are present with equal amplitudes. To make this clear, consider two time series generated from

$$[\mathbf{u}_1(t)\ \mathbf{u}_2(t)] = \boldsymbol{\xi}_1(t)\frac{1}{\sqrt{2}}[1\ 1] + \boldsymbol{\xi}_2(t)\frac{1}{\sqrt{2}}[1\ -1] \quad \text{(A3)}$$

so that there is rigorous vertical orthogonality, but only statistical orthogonality in time. But the EOFs of (A3) produce

$$[\mathbf{u}_1(t)\ \mathbf{u}_2(t)] = \lambda_1\boldsymbol{\alpha}_1(t)[0.170\ .986] + \lambda_2\boldsymbol{\alpha}_2(t)[0.986\ -0.170], \quad \text{(A4)}$$

$$\lambda_1 = 20.3, \qquad \lambda_2 = 18.4, \quad \text{(A5)}$$

where a different orthogonal basis has emerged—the result of technical details of the SVD (eigenvalue) code and the lack of perfect orthogonality in time. Necessarily, the new vertical modes $\boldsymbol{\alpha}_1$, $\boldsymbol{\alpha}_2$ are linear combinations of the original orthogonal bases.

There are two clues here to this problem. The first is that the two singular values are very close in numerical values, and the vertical structures of the two EOFs are intimately connected (although a two-point vertical structure does not show this clearly).

If the synthetic example is changed to

$$[\mathbf{u}_1(t)\ \mathbf{u}_2(t)] = \boldsymbol{\xi}_1(t)\frac{1}{\sqrt{2}}[1\ 1] + \boldsymbol{\xi}_2(t)\frac{1/10}{\sqrt{2}}[1\ -1] \quad \text{(A6)}$$

so that the second structure has only 1% of the energy of the first, the SVD produces

$$[\mathbf{u}_1(t)\ \mathbf{u}_2(t)] = \alpha_1(t)\lambda_1[0.701\ 0.713] + \alpha_2(t)\lambda_2[-0.713\ 0.701], \quad \text{(A7)}$$

$$\lambda_1 = 19.7, \qquad \lambda_2 = 1.90, \quad \text{(A8)}$$

a nearly perfect result: The dominance of the first mode preventing ambiguity in the construction of the dominant EOF.

If the first EOF is clearly dominant, then one is entitled to conclude that there is a unique lowest mode. To avoid these problems, we prefer in this paper to use the linear mode fits and then to estimate the degree of correlation (or coherence) between the coefficients. Additionally, as noted above, the dynamical modes readily lend themselves to a surface extrapolation—necessary with measurements that are typically hundreds of meters below the sea surface, and the EOFs cannot be extrapolated beyond the uppermost measurement.

The EOFs are useful, however, for confirming the breakdown of the statistical partitioning hypothesis. For example, Fig. A2 displays the EOFs for u, v from a mooring in the Brazil Basin. The anomalous structure at depth is apparent.

APPENDIX B

Percentage Confidence Limits

We need an estimate of the reliability of the modal decompositions. The basic statistical result is found in Eq. (6) for $\mathbf{P}_u(1)$, $\mathbf{P}_v(1)$, which are the uncertainties of $\overline{\boldsymbol{\alpha}}_u$, $\overline{\boldsymbol{\alpha}}_v$ respectively. The percentages of the modal fits are in the form

$$g_i = \frac{\langle\tilde{\alpha}_i^2\rangle_L}{\sum_{j=1}^{N}\langle\tilde{\alpha}_j^2\rangle_L}, \quad \text{(B1)}$$

where the bracket denotes the sample mean over L estimates of the squared coefficient, and a confidence limit for g_i is sought. Define $\tilde{x}_i^2 = \langle\tilde{\alpha}_i^2\rangle_L$, where x_i is approximately Gaussian. It can be shown (J. B. Keller and A. S. Whittemore 1996, personal communication) that

$$f_i = \log\left(\frac{g_i}{1-g_i}\right) \quad \text{(B2)}$$

will be approximately Gaussian with variance

$$\mathrm{var}(f_i) = \mathrm{cov}(f)_{ii} = \frac{4}{x_i^2}\mathbf{P}(1)_{ii} + \frac{4}{x_i}\sum_{j\neq i}\mathbf{P}(1)_{ij}\frac{(-2x_j)}{\sum_{k\neq i}x_k^2} + \sum_{\substack{s\neq i\\ j\neq i}}\frac{(-2x_s)\mathbf{P}(1)_{sj}(-2x_j)}{\left(\sum_{k\neq i}x_k^2\right)^2}, \quad \text{(B3)}$$

and the u, v subscripts have been suppressed. An approximate 95% confidence interval for g_i is

$$\frac{\exp\{x_i - 1.96\ \mathrm{var}(f_i)^{1/2}\}}{1+\exp\{x_i - 1.96\ \mathrm{var}(f_i)^{1/2}\}} < g_i < \frac{\exp\{x_i + 1.96\ \mathrm{var}(f_i)^{1/2}\}}{1+\exp\{x_i + 1.96\ \mathrm{var}(f_i)^{1/2}\}}. \quad \text{(B4)}$$

The estimated value, $\tilde{x}_i = 0$ is employed everywhere that the true value x_i appears in (B3), (B4). These results

are approximate for a number of reasons, including the rough measure of $\mathbf{P}(1)$.

The result in Eq. (B4) was tabulated for each mode on each mooring using the estimated $\mathbf{P}(1)$ from Eq. (6). Although these are not displayed, and the results not entirely consistent with the estimated percentages [owing, it is believed, to the approximate nature of $\mathbf{P}(1)$], the general patterns are readily summarized. For the 10 instrument mooring (No. 31), the confidence interval for the barotropic and first baroclinic modes are quite small (range of about 4%), growing to a range of about 15% for the fourth baroclinic mode. In contrast, the many three instrument moorings of the western Pacific have a barotropic mode confidence limit approaching 100%, while the first baroclinic mode is determined within about 20%. Higher mode confidence limits again approach 100%. Thus, the contourable patterns are, as asserted above, largely the result of using many results—few of which individually are of significance.

The Brazil Basin moorings, which appear anomalous, have confidence limits approaching 100% for all modes—a consequence of the vertical instrument distribution.

REFERENCES

Arhan, M., A. Colin de Verdière, and H. Mercier, 1989: Direct observations of the mean circulation at 48°N in the Atlantic Ocean. *J. Phys. Oceanogr.,* **19,** 161–181.

Bower, A. S., and N. G. Hogg, 1996: Structure of the Gulf Stream and its recirculation at 55°W. *J. Phys. Oceanogr.,* **26,** 1002–1022.

Brink, K., 1995: Tidal and lower frequency currents above Fieberling Guyot. *J. Geophys. Res.,* **100,** 10 817–10 832.

Brügge, B., 1995: Near-surface mean circulation and kinetic energy in the central North Atlantic from drifter data. *J. Geophys. Res.,* **100,** 20 543–20 554.

Chechelnitsky, M., 1996: Global barotropic variability of the ocean in response to atmospheric forcing based on multichannel regression and Kalman filter techniques, S.M. thesis, MIT/WHOI Joint Program, 112 pp.

Colin de Verdière, A., H. Mercier, and M. Arhan, 1989: Mesoscale variability transition from the western to the eastern Atlantic along 48°. *J. Phys. Oceanogr.,* **19,** 1149–1170.

Davis, R. E., 1975: Statistical methods. Dynamics and the analysis of MODE-I: Rep. of the MODE-I Dynamics Group, Dept. of Meteorology, MIT, Cambridge, 250 pp.

Dickson, R. R., 1989: Flow statistics from long-term current-meter moorings. The global data-set in January 1989. World Ocean Circulation Experiment, WCRP-30, WMO/TD-No. 337, World Climate Research Program, 35 pp. plus numerous tables. [Available from International WOCE Project Office, Southampton Oceanography Centre, Southampton 5014 3ZH, United Kingdom.]

Eriksen, C., 1985: Some characteristics of internal gravity waves in the equatorial Pacific. *J. Geophys. Res.,* **90,** 7243–7255.

Fofonoff, N. P., and R. M. Hendry, 1985: Current variability near the southeast Newfoundland ridge. *J. Phys. Oceanogr.,* **15,** 963–984.

Fu, L.-L., and R. A. Davidson, 1995: A note on the barotropic response of sea level to time-dependent wind forcing. *J. Geophys. Res.,* **100,** 24 955–24 963.

——, T. Keffer, P. Niiler, and C. Wunsch, 1982: Observations of mesoscale variability in the western North Atlantic: A comparative study. *J. Mar. Res.,* **40,** 809–848.

Garzoli, S., A. L. Gordon, V. Kamenkovich, D. Pillsbury, and C. Duncombe-Rae, 1996: Variability and sources of the southeastern Atlantic circulation. *J. Mar. Res.,* **54,** 1039–1071.

Gaspar, P., and C. Wunsch, 1989: Estimates from altimeter data of barotropic Rossby waves in the northwestern Atlantic Ocean. *J. Phys. Oceanogr.,* **19,** 1821–1844.

Gill, A. E., 1982: *Atmosphere–Ocean Dynamics.* Academic Press, 662 pp.

——, J. S. A. Green, and A. J. Simmons, 1974: Energy partition in the large-scale ocean circulation and the production of mid-ocean eddies. *Deep-Sea Res.,* **21,** 499–528.

Gould, W. J., 1983: The northeast Atlantic Ocean. *Eddies in Marine Science,* A. R. Robinson, Ed., Springer-Verlag, 145–157.

Hamann, I., and B. A. Taft, 1987: The Kuroshio Extension near the Emperor Seamounts. *J. Geophys. Res.,* **92,** 3827–3839.

Hogg, N. G., R. S. Pickart, R. M. Hendry, and W. J. Smethie Jr. 1986: The northern recirculation gyre of the Gulf Stream. *Deep-Sea Res.,* **33,** 1139–1165.

——, W. B. Owens, G. Siedler, and W. Zenk 1996: Circulation in the deep Brazil Basin. *The South Atlantic: Past and Present Circulation,* G. Wefer, W. H. Berger, G. Siedler, and D. Webb, Eds., Springer-Verlag, in press.

Inoue, M., 1985: Modal decomposition of low-frequency currents and baroclinic instability at Drake Passage. *J. Phys. Oceanogr.,* **15,** 1157–1181.

Jolliffe, I. T., 1986: *Principal Component Analysis.* Springer-Verlag, 271 pp.

Kotz, S., and N. C. Johnson, Eds., 1985: *Encyclopedia of Statistical Sciences.* Vol. 5, Wiley, 741 pp.

Levitus, S., and T. P. Boyer, 1994: *World Ocean Atlas 1994.* Vol. 4, *Temperature,* NOAA Atlas NESDIS 4, U.S. Gov. Printing Office, 117 pp.,

Liebelt, P. B., 1967: *An Introduction to Optimal Estimation.* Addison-Wesley, 273 pp.

Lippert, A., and M. G. Briscoe, 1990: Observations and EOF analysis of low-frequency variability in the western part of the Gulf Stream recirculation. *J. Phys. Oceanogr.,* **20,** 646–656.

Luyten, J. R., M. Fieux, and J. Gonella, 1980: Equatorial currents in the western Indian Ocean. *Science,* **209,** 600–603.

——, A. Spencer, S. Tarbell, K. Luetkemeyer, P. Flament, J. Toole, M. Francis, and S. Bennett, 1990: Moored currentmeter, AVHRR, CTD, and drifter data from the Agulhas Current and retroflexion region (1985–1987) Volume XLII. Tech. Rep. 90-30, WHOI, 100 pp. and insert. [Available from Reference Librarian, Woods Hole Oceanographic Institution, Woods Hole, MA 02540.]

McWilliams, J. C., 1976: Maps from the Mid-Ocean Dynamics Experiment: I. Geostrophic stream function. *J. Phys. Oceanogr.,* **6,** 810–827.

——, and C. Y. Shen, 1980: Mesoscale modal coupling. *J. Phys. Oceanogr.,* **10,** 741–752.

Mercier, H., and A. Colin de Verdière, 1985: Space and time scales of mesoscale motions in the eastern North Atlantic. *J. Phys. Oceanogr.,* **15,** 171–183.

Müller, T. J., and G. Siedler, 1992: Multi-year current time series in the eastern North Atlantic Ocean. *J. Mar. Res.,* **50,** 63–98.

Niiler, P. P., and M. M. Hall, 1988: Low-frequency eddy variability at 28°N, 152°W in the eastern North Pacific subtropical gyre. *J. Phys Oceanogr.,* **18,** 1670–1685.

Picaut, J., and L. Sombardier, 1993: Influence of density stratification and both depth on vertical mode structure functions in the tropical Pacific. *J. Geophys. Res.,* **98,** 14 727–14 737.

Pillsbury, R. D., D. Barstow, B. Moore, G. Pittock, D. C. Root, J. Simpkins III, and R. E. Still, 1985: Data report for current meters on mooring Nares-1, 1983–84; Nares abyssal plain. Contractor Rep. SAND85-7215, 110 pp. [Available from Sandia National Laboratories, P.O. Box 5800, Albuquerque, NM 87185.]

Priestley, M. B., 1981: *Spectral Analysis and Time Series,* Vol. 1, *Univariate Series*; Vol. 2, *Multivariate Series, Prediction and Control.* Academic Press, 890 pp plus appendices.

Richardson, P. L., 1983: Eddy kinetic energy in the North Atlantic from surface drifters. *J. Geophys. Res.,* **88,** 4355–4367.

Richman, J., C. Wunsch, and N. Hogg, 1977: Space and time scales of meso-scale motion in the western North Atlantic. *Rev. Geophys. Space Phys.,* **15,** 385–420.

Schmitz, W. J., Jr., 1988: Exploration of the eddy field in the mid-latitude North Pacific. *J. Phys. Oceanogr.,* **18** 459–468.

——, 1989: The MODE site revisited. *J. Mar. Res.,* **45,** 131–151.

——, and J. R. Luyten, 1991: Spectral time scales for mid-latitude eddies. *J. Mar. Res.,* **49,** 75–107.

Shay, T. J., J. M. Bane, D. R. Watts, and K. L. Tracey, 1995: Gulf Stream flow field and events near 68°W. *J. Geophys. Res.,* **100,** 22 565–22 589.

Stammer, D., 1997: Global characteristics of ocean variability estimated from regional TOPEX/POSEIDON altimeter measurements. *J. Phys. Oceanogr,* **27,** 1743–1769.

——, R. Tokmakian, A. Semtner, and C. Wunsch, 1996: How closely does a 1/4° global ocean circulation model simulate large-scale observations? *J. Geophys. Res.,* **101,** 25 779–25 811.

Wallace, J. M., 1972: Empirical orthogonal representation of time series in the frequency domain. Part II: Application to the study of tropical wave disturbances. *J. Appl. Meteor.,* **11,** 893–900.

White, M. A., and K. J. Heywood, 1995: Seasonal and interannual changes in the North Atlantic subpolar gyre from GEOSAT and TOPEX/POSEIDON altimetry. *J. Geophys. Res.,* **100,** 24 931–24 941.

Whitworth, T., III, W. D. Nowlin Jr., R. D. Pillsbury, M. I. Moore, and R. F. Weiss, 1991: Observations of the Antarctic circumpolar current and deep boundary current in the Southwest Atlantic. *J. Geophys. Res.,* **96,** 15 105–15 118.

Woodgate, R. A., and P. D. Killworth, 1996: The problem of the barotropic mode in deriving pressure from density by using vertical normal modes. *J. Geophys. Res.,* **101,** 3765–3768.

Wunsch, C., 1996: *The Ocean Circulation Inverse Problem.* Cambridge University Press, 437 pp.

——, and D. Stammer, 1995: The global frequency-wavenumber spectrum of oceanic variability estimated from TOPEX/POSEIDON altimetric measurements. *J. Geophys. Res.,* **100,** 24 895–24 910

——, and ——, 1997: Atmospheric loading and the ''inverted barometer'' effect. *Revs. Geophys.,* **35,** 79–107.